Identification of Mebendazole as an ethylene signaling activator reveals a role of ethylene signaling in the regulation of lateral root angles

Wenrong He1, Hai An Truong 1, Ling Zhang 1, Min Cao 1, Neal Arakawa 3, Yao Xiao 4, Kaizhen Zhong1, Yingnan Hou 5, 6, Wolfgang Busch1,2,7

1. Plant Molecular and Cellular Biology Laboratory, Salk Institute for Biological Studies, La Jolla, California, USA
2. Integrative Biology Laboratory, Salk Institute for Biological Studies, La Jolla, California, USA
3. Environmental and Complex Analysis Laboratory (ECAL), Department of Chemistry and Biochemistry, University of California, San Diego, La Jolla, USA
4. Department of Integrative Structural and Computational Biology, The Scripps Research Institute, La Jolla, California, USA
5. Department of Microbiology and Plant Pathology, Center for Plant Cell Biology, University of California, Riverside, California, USA
6. School of Agriculture and Biology, Shanghai Jiao Tong University, Shanghai, China
7. Lead contact

Correspondence: wbusch@salk.edu

In brief: He *et al.* identify a small molecule that regulates lateral root angle. They show that the compound increases lateral root angle by inhibiting CTR1 kinase activity, which in turn activates ethylene signaling. Therefore, they uncover that the ethylene pathway is involved in lateral root angle regulation.

Highlights:

- MBZ increases lateral root angle
- MBZ regulates lateral root angle by activating ethylene signaling
- MBZ inhibits CTR1 kinase activity
- The ethylene pathway is involved in lateral root angle regulation

SUMMARY

The lateral root angle or gravitropic set-point angle (GSA) is an important trait for root system architecture (RSA) that determines the radial expansion of the root system. The GSA therefore plays a crucial role for the ability of plants to access nutrients and water in the soil. Despite its importance, only few regulatory pathways and mechanisms that determine GSA are known, and these mostly relate to auxin and cytokinin pathways. Here, we report the identification of a small molecule, Mebendazole (MBZ) that modulates GSA in *Arabidopsis thaliana* roots and acts via the activation of ethylene signaling. We uncover that MBZ directly acts on the serine/threonine protein kinase CTR1, which is a negative regulator of ethylene signaling. Our study not only reveals that the ethylene signaling pathway is essential for GSA regulation, but it also identifies a small molecular modulator of RSA and the first small molecule that acts downstream of ethylene receptors and that directly activates ethylene signaling.

KEYWORDS

Root System Architecture, Lateral Root Angle, Root Growth, Ethylene Signaling, Chemical genetics, Mebendazole

INTRODUCTION

The root systems of plants are vital for plant survival and productivity. They anchor plants and they absorb water and nutrients from the soil. The distribution of roots in the soil, root system architecture (RSA), is of enormous relevance. For instance, deeper rooting is associated with higher carbon permanence (Poirier et al., 2018), a critical trait for soil carbon sequestration and the ability of plants to survive terminal droughts (Uga et al., 2013). Besides, to enhance the capacity for root systems to efficiently uptake nitrogen and water, deeper roots are required, yet for improving the uptake of phosphate and other nutrients, shallower soil layers have to be accessed by roots (Lynch, 2019). A key determinant of RSA is the lateral root angle or gravitropic set-point angle (GSA). Previous studies have shown that auxin plays a crucial role in regulating GSA (Rosquete et al., 2013a; Roychoudhry et al., 2013; Xiao and Zhang, 2020). Application of exogenous IAA or synthetic auxin leads to lateral root growth toward the vector of gravity thereby

decreasing GSA (Rosquete et al., 2013a; Roychoudhry et al., 2013). Another phytohormone, cytokinin, was also found to be involved in the regulation of GSA. Application of cytokinin showed an anti-gravitropic effect and thereby increased GSA (Waidmann et al., 2019b). Finally, members of the IGT gene family, including DRO1/LAZY4 have been shown to play a major role in lateral root angles via auxin associated mechanisms (Ge and Chen, 2016; Guseman et al., 2017; Waite and Dardick, 2021; Yoshihara and Spalding, 2017).

Ethylene is an ancient plant hormone. The ethylene signaling pathway is highly conserved and was present already in the aquatic progenitors of land plants (Ju et al., 2015). Ethylene is produced from the conversion of S-adenosyl-L-methionine (SAM) to 1-aminocy-clopropane-1-carboxylic acid (ACC) and then to ethylene, which is catalyzed by enzymes including ACC synthase (ACS) and ACC oxidase (ACO) (Pattyn et al., 2021; S F Yang and Hoffman, 1984). When ethylene binds to its receptors (ETRs) (Chang et al., 1993; Hua et al., 1998; Sakai et al., 1998), it inactivates a serine/threonine protein kinase, CONSTITUTIVE TRIPLE RESPONSE1(CTR1) (Kieber et al., 1993). In the absence of ethylene, CTR1 blocks ethylene downstream responses by phosphorylating the C-terminal end of ETHYLENE-INSENSITIVE2 (EIN2), an ER–associated membrane protein that works as a positive regulator of ethylene signaling (Alonso et al., 1999; Ju et al., 2012; Wen et al., 2012). This leads to the degradation of EIN2-CEND by the Ub/26S proteasome (Ju et al., 2012; Qiao et al., 2012a; Wen et al., 2012). When CTR1 is inactivated by ethylene binding to ETRs, EIN2-CEND is stabilized and moves into the nucleus to transduce the ethylene signal to downstream transcription factors, such as EIN3, EIN3 LIKE1 (EIL1) (An et al., 2010; Chao et al., 1997) and ETHYLENE RESPONSE FACTORs (ERFs) (Muller and Munne-Bosch, 2015). These transcription factors activate the downstream ethylene response. The ethylene pathway was found to play an important role in numerous growth and developmental processes in the root, such as the inhibition of root elongation (Kieber et al., 1993; Le et al., 2001; Vaseva et al., 2018), induction of root hair growth (Feng et al., 2017), and inhibition of the initiation of lateral roots (LRs) (Negi et al., 2008).

96 To identify potential regulators of GSA, we performed a chemical genetics screen and
97 identified a small molecule, Mebendazole (MBZ), which dramatically increased GSA.
98 Genetic analysis revealed that MBZ increased GSA through rapidly activating the
99 ethylene signaling pathway. Both MBZ and ACC treatment induced ethylene signaling,
100 which led to a modulation of lateral root angle. Further molecular and biochemistry studies
101 showed that MBZ activates ethylene signaling by specifically targeting CTR1 and thereby
102 blocking its kinase activity. Our study not only identified MBZ as an efficient small
103 molecular activator of ethylene signaling, but also uncovered that ethylene signaling plays
104 an important role in regulating GSA.
105
106 **Results**
107 **A small compound profoundly affects the lateral root gravitropic set-point angle**
108 **(GSA) in Arabidopsis**
109 To identify small molecules that affect GSA, we screened chemicals for their ability to
110 change GSA of young seedlings from a small molecular library with 2000 diverse generic
111 chemicals (SP 2000)(He et al., 2011; Sun et al., 2017; Zhu et al., 2019). We found that
112 treatment with Mebendazole (MBZ) (Figure S1A) led to a distinct increase of lateral root
113 angles that caused lateral roots to grow in a more horizontal direction (Figure 1A). The
114 lateral root GSA of untreated two-week-old Arabidopsis seedlings was approx. 46°, and
115 the GSA of lateral roots of seedlings grown on 1 μM MBZ plates was approx. 70° (Figure
116 1A, B). While the lateral root angle was the most striking phenotype, at a much earlier
117 developmental stage (one week after germination), seedlings on 1 μM MBZ displayed a
118 decreased root length (in average reduced by 37%) and an increased root hair initiation
119 and elongation (Figure 1C, D, Figure S1B, C). To test how quickly MBZ would affect
120 lateral root growth, we grew seedlings for 14 days on ½ MS medium with DMSO, then
121 transferred them to ½ MS medium supplemented with 1 μM MBZ and acquired images
122 every 10 minutes. All of the 5 measured lateral root tips started to grow at a more
123 horizontal (less steep) angle within 3 hours of MBZ treatment (Figure 1E upper panel, F),
124 which coincided with the first timepoint at which root angles were significantly different
125 between control and MBZ (Welch Two Sample t-test; p-value <0.05). To test whether the
126 action of MBZ was reversible, we germinated and grew seedlings on ½ MS for 5 days,

127 and then transferred them to medium containing 1 μM MBZ for 14 days, thereby inducing
128 lateral roots of MBZ treated seedlings to grow more horizontally. We note that we used
129 this later timepoint (compared to the data presented in the upper panel) to be able to
130 consider enough lateral roots that were growing at the more horizontal angle. We then
131 transferred the seedlings back to control conditions and acquired images every 10
132 minutes. Already after one hour root angles were significantly different between control
133 (MBZ) and treatment (removal from MBZ) conditions (Welch Two Sample t-test; p-value
134 <0.05), and within 4 hours all 5 lateral root tips we measured started to grow at a distinctly
135 steeper angle upon removal from MBZ (Figure 1E bottom panel, F). These data showed
136 that the treatment of Arabidopsis roots with MBZ changes lateral root angles within 3
137 hours and that this effect is fully reversible. In summary, we found that MBZ changes
138 lateral root angles and important RSA traits associated with the development of a shallow
139 root system.
140
141 **Application of MBZ induces the ethylene pathway**
142 To identify the pathway that MBZ acted upon, we utilized a genome-scale expression
143 profiling approach. For this, we performed an mRNA-seq experiment using whole roots
144 of 14-day-old Arabidopsis grown on ½ MS media treated with 10 μM MBZ for 4 hours.
145 The analysis revealed that 677 genes were induced compared to mock treatment
146 (FDR<0.05; log2 fold change > 1) and 658 genes were repressed (FDR<0.05; log2 fold
147 change < -1). A gene ontology (GO) analysis revealed that among the genes that were
148 upregulated by MBZ, genes involved in ethylene responses were strongly
149 overrepresented in this early response. In particular, the GO process “negative regulation
150 of ethylene-activated signaling pathway” (GO:0010105) was the most enriched process
151 (~21 fold enrichment, P-value: $6.07*10^{-4}$) upon MBZ treatment (Figure 2A), and the 4th
152 most enriched GO process was “ethylene-activated signaling pathway” (GO:0009873)
153 (~11 fold enrichment, P-value:$7.45*10^{-5}$) (Figure 2A). Other GO categories were also
154 significantly enriched, most notably responses to light. However, given that ethylene
155 signaling was the most enriched GO term, we first looked at the responses of genes
156 involved in the ethylene hormone pathway. A major portion of these genes were
157 differentially regulated by MBZ compared to mock treatment (Figure 2A, B). We therefore

158 hypothesized that MBZ elicited the ethylene pathway. To test this hypothesis, we first
159 compared the set of genes that had responded to MBZ with a published transcriptome
160 dataset that had been generated by exposing roots to 4 hours of ethylene treatment
161 (Chang et al., 2013). Of the 1335 differentially expressed genes (DEGs) upon the 4 hours
162 of MBZ treatment, 306 were overlapping with 1397 DEGs upon 4 hours of ethylene
163 treatment (P-value for the overlap using a hypergeometric test: $p < 4.657*10^{-143}$) (Figure
164 S3A). Notably, more than 90% of these common DEGs retained the directionality of their
165 expression change (i.e. genes upregulated by MBZ were also upregulated by ethylene
166 treatment and vice versa) (Figure S3B, C). While this overlap was highly significant and
167 supported the hypothesis that MBZ elicited ethylene responses, there was a high number
168 of differentially expressed genes that didn't overlap. We reasoned that this might be due
169 to differences in developmental and growth conditions of our MBZ-treated plants and of
170 those plants used for the published ethylene treatment dataset (Chang et al., 2013). For
171 instance, we had used 14-day-old seedlings grown under long day conditions before we
172 conducted the treatment and the published data had utilized 3-day-old, dark-grown
173 seedlings for eliciting the classical ethylene triple response phenotype. To compare
174 ethylene responses to MBZ responses under the same growth conditions and plant age,
175 we performed another mRNA-seq experiment using roots of 14-day-old Arabidopsis
176 grown on ½ MS media treated with 10 µM MBZ or 10 µM ACC (the ethylene precursor)
177 for 3 hours. We then again compared the overlap of the responsive genes. Out of 826
178 DEGs upon the MBZ treatment, 524 were overlapping with 741 DEGs upon 3 hours of
179 ACC treatment, accounting for 63 and 71% of DEGs upon MBZ and ACC treatment
180 respectively (Figure 2C). 77% upregulated DEGs of the MBZ treatment overlapped with
181 65% upregulated DEGs of the ACC treatment (Figure 2D). These fractions were 54% and
182 75% for downregulated DEGs (Figure 2E). Taken together, our data strongly suggested
183 that application of MBZ induces the ethylene pathway but in addition might also elicit non-
184 ethylene related effects.
185
186 **MBZ induces ethylene responses**
187 To investigate how MBZ treatment effects the ethylene response, we compared plant
188 responses to MBZ and the ethylene precursor ACC. The most characteristic response to

189 ethylene treatment is the triple response of etiolated seedlings (Guzman and Ecker, 1990)
190 (Figure 3A to C), which includes shortened and thickened roots and hypocotyls, and an
191 exaggerated apical hook. Consistent with our hypothesis that MBZ activates ethylene
192 responses, 3-day-old etiolated seedlings treated with 10 μM MBZ showed a prominent
193 triple response phenotype (Figure 3A to C). Using different doses of MBZ, we found that
194 2.5 μM of MBZ was sufficient to induce the triple response phenotype in a dark
195 environment (Figure S3A to F), we therefore started to use 2.5 μM of MBZ to observe
196 triple responses. Consistent with MBZ mimicking ethylene treatment, MBZ induced triple
197 response was abolished in the ethylene insensitive mutants *ein2-5* and *ein3 eil1* (Figure
198 S3D to F). Ethylene treatment inhibits root elongation mainly by repressing cell elongation
199 rather than reducing the length of meristem (De Cnodder et al., 2005; Vaseva et al., 2018).
200 We therefore measured the length of root cells of 4-day-old etiolated seedlings treated
201 with 2.5 μM MBZ and 10 μM ACC, and found that similar to the ACC treatment, the mature
202 cell size was reduced by MBZ treatment (Figure 3D to F). Altogether, our data strongly
203 suggested that MBZ elicits its effects via the ethylene pathway.
204 As we wanted to identify the mechanism by which MBZ changes the steepness of lateral
205 root angles and given our data that MBZ acts on the ethylene pathway, we conducted an
206 RNA-seq experiment on lateral root tips that had been treated either with DMSO or MBZ
207 for 3 hours. As sample collection was very challenging and took an hour per replicate, the
208 sampled lateral roots had been treated for a time between 3-4 hours. The most enriched
209 gene ontology categories were “regulation of transcription”, “response to auxin”, “ethylene
210 activated signaling pathway” and “cytokinin-signaling pathway" (Figure 2F). Given that
211 the time window for the RNA-seq coincided with the change of lateral root angle, it was
212 not surprising to detect auxin and cytokinin related genes, as these two hormonal
213 pathways had been shown to be involved in determining the GSA of lateral roots
214 (Rosquete et al., 2013a; Roychoudhry et al., 2013; Waidmann et al., 2019b). However,
215 given the enrichment of genes assigned to these pathways we wanted to check whether
216 these pathways are activated before or after ethylene responses were elicited by MBZ.
217 To do this, we obtained the *DR5-GFP V2* auxin response reporter line (Liao et al., 2015a),
218 the *35S-EIN3-GFP* ethylene reporter line in the *ein3 eil1* background (He et al., 2011),
219 and the *TCN-GFP* cytokinin reporter line (Zurcher et al., 2013). We then conducted time-

220 lapse spinning disk confocal microscopy on lateral root tips from 14-day-old seedlings
221 that were either treated with a DMSO control solution, MBZ, or the respective positive
222 control (the auxin IAA, the cytokinin Zeatin, or the ethylene precursor ACC). All positive
223 control treatments swiftly induced the expression of the reporter genes in lateral roots
224 (Figure 2G-L; Suppl. Movies 1, 3, 4, 6, 7, 9). Consistent with our hypothesis that MBZ
225 induced the ethylene pathway, MBZ treatment drastically induced the ethylene reporter
226 within the first 20 minutes after treatment, even before the ethylene precursor ACC
227 induced the reporter (Figure 2G, J; Suppl. Movies 1-3). MBZ treatment did not lead to an
228 increased signal of the auxin response reporter, while the DMSO control led to a slight
229 decrease of the reporter signal after 40 minutes, and the IAA treatment led to a strong
230 increase throughout the whole duration of the experiment (Figure 2H, K; Suppl. Movies
231 4-6). There was no induction of the cytokinin reporter by MBZ in the timeframe we
232 observed the roots (Figure 2I, L; Suppl. Movies 7-9). Overall, these data strongly
233 suggested that MBZ strongly and swiftly induces the ethylene pathway in lateral root tips.
234

235 **MBZ activates ethylene signaling**

236 Next, we set out to locate the target of MBZ in the ethylene pathway. First, we tested
237 whether MBZ induces ethylene biosynthesis, or acts on the perception of ethylene, or on
238 the ethylene signaling pathway. To test whether ethylene biosynthesis is affected, we
239 measured ethylene production by GC-MS in 3-day-old etiolated Col-0 seedlings that were
240 treated with 10 µM MBZ or ACC. Ethylene production was dramatically induced by 10 µM
241 ACC, but not detected in DMSO or 10 µM MBZ-treated-seedlings (Figure 4A). The results
242 suggested that MBZ acts downstream of ethylene biosynthesis. To further test this
243 hypothesis, we utilized gain-of-function mutants in the ethylene receptor *ETR1*. Root
244 growth and GSA in strong *ETR1* alleles *etr1-1 and etr1-3,* were still strongly altered upon
245 MBZ treatment (Figure 4B to E). Moreover, 4-day-old etiolated seedlings of *etr1-3* treated
246 with 2.5 µM MBZ showed the typical triple response phenotype, demonstrating that
247 ethylene responses are triggered by MBZ even without induced ethylene production or
248 the perception of ethylene by ETR1 (Figure S3A to C). In contrast to the response to MBZ,
249 *etr1-3* plants were completely insensitive to the treatment with 10 µM of ACC (Figure S3A

250 to C). Collectively, these results show that MBZ induces ethylene responses by targeting
251 factors downstream of ethylene biosynthesis and perception.
252 To uncover which components of ethylene signaling are targeted by MBZ, we studied
253 MBZ responses in key mutants of the ethylene signaling pathway. First, we checked the
254 root inhibition phenotype and GSA in *ctr1-1* mutant treated with MBZ and compared these
255 responses to the Col-0 wild type. *CTR1* is the first negative regulator of ethylene signaling
256 acting downstream of ethylene receptors, and *EIN2* and *EIN3/EIL1* are positive regulators
257 that act downstream of *CTR1* to trigger ethylene signaling (Figure 5A). Roots of Col-0
258 were sensitive to 1.2 μM MBZ treatment and showed short roots and increased root hair
259 development (Figure 5B, C). However, *ctr1-1* mutants in which ethylene signaling is
260 constitutively active showed short roots and abundant root hairs without any treatment at
261 an early stage. Due to this pronounced early-seedling phenotype, we could not
262 confidently assess changes in response to MBZ. However, we noticed that root growth
263 remained insensitive to MBZ (Figure 5B, C). We further measured GSA at a later stage
264 of development, which we had found to be a major effect of MBZ treatment. 3-week-old
265 *ctr1-1* plants were insensitive to MBZ with regards to GSA (Figure 5D, E). Interestingly,
266 *ctr1-1* without MBZ treatment showed an increased lateral root angle phenotype, which
267 mimics MBZ treatment, suggesting that CTR1 might be the target of MBZ in ethylene
268 signaling. Consistent with this hypothesis, root growth and GSA of *ein2-5* and *ein3 eil1*
269 was clearly not affected by MBZ treatment (Figure 5B, C, F, G) and in fact, *ein2-5* mutant
270 plants, which are insensitive to ethylene, displayed steeper lateral root angles under
271 control conditions compared to the wildtype (Figure 5F, G). We further tested triple
272 responses in *ctr1-1*, *ein2-5* and *ein3 eil1* mutants. Consistent with the observation of root
273 inhibition and GSA in *ctr1-1*, these plants showed a constitutive triple response regardless
274 of MBZ treatment (Figure S3D to F). *ein2-5* and *ein3 eil1* plants were also insensitive to
275 MBZ treatment (Figure S3D to F). Taken together our data showed that MBZ activates
276 ethylene signaling most likely by interfering with CTR1 in the ethylene signaling pathway.
277
278 **MBZ is a potent inhibitor of CTR1 kinase activity**
279 To pinpoint whether CTR1 is the target of MBZ, we capitalized on what is known about
280 the activity of MBZ in mammalian systems. There, MBZ has been reported to be an

281 inhibitor of the serine/threonine kinase *homo sapiens* (*hs*) MAPK14 (Ariey-Bonnet et al.,
282 2020). Because CTR1 is also a serine/threonine protein kinase (Kieber et al., 1993), we
283 hypothesized that CTR1 is the direct target of MBZ in plants. Since it was shown that
284 there are four critical amino acid residues in the catalytic site of *hs*MAPK14 that are
285 relevant for MBZ binding (Ariey-Bonnet et al., 2020), we first tested *in silico* whether these
286 residues were conserved between *hs*MAPK14 and CTR1. For this, we aligned the amino
287 acid sequence of the Arabidopsis CTR1 and *hs*MAPK14 kinase domains (Figure 6A,
288 Figure S4A, B). We found three (Lys 578, Thr 625, and Asp 694) of the four critical amino
289 acid residues were conserved between the CTR1 kinase domain and that of *hs*MAPK14
290 (Figure 6A). The 4th critical residue is Met 109 in *hs*MAPK14, which corresponds to Leu
291 628 in CTR1. Because both Met and Leu are non-polar amino acids with hydrophobic
292 side chains and similar structure, it appeared possible that the replacement of Met by Leu
293 in the CTR1 kinase domain does not significantly change the pocket structure for MBZ
294 binding. We therefore hypothesized that the kinase domains of CTR1 and MAPK14 might
295 have similar structures and function with regards to binding MBZ (Figure S4B).
296 To test this hypothesis, we first performed an *in silico* docking analysis using the published
297 crystal structures of CTR1 (Mayerhofer et al., 2012)(PDB: 3PPZ) and MBZ (CHEMBL685).
298 We found that MBZ is predicted to bind into the pocket of the CTR1 kinase domain (Figure
299 6B) formed by the aforementioned key amino acids (Figure 6A, B, Figure S4B). Overall,
300 these analyses indicated that CTR1 could be the target of MBZ in Arabidopsis.
301 To further test this model, we expressed the recombinant kinase domains (KD) of CTR1
302 and MAPK4 (a MAPK protein in Arabidopsis with a highly similar amino acid sequence to
303 *hs*MAPK14) (Table S1, Figure S4C, D). We then confirmed the kinase inhibitory activity
304 of MBZ through an *in vitro* phosphorylation assay via anti-Thiophosphate-Ester antibodies
305 (Allen et al., 2007). Using the phosphorylation state of MBP (substrate) as the readout of
306 the kinase activity, we found that MBZ inhibited the kinase activities of both CTR1-KD
307 and MPK4 in a concentration-dependent manner, however, the inhibition for CTR1-KD
308 was much more pronounced (Figure 6C, D). In particular, 10 μM MBZ strongly inhibited
309 the kinase activity of CTR1-KD, while 100 μM MBZ totally blocked its activity. This assay
310 demonstrated that MBZ can directly inhibit the kinase activity of CTR1-KD. Together with
311 our genetic data that *ctr1-1* mutant mimicked the effect of MBZ on GSA and the triple

312 response phenotypes (Figure 5D, E, Figure S3D-F), and our molecular docking data
313 (Figure 6B), our data strongly suggest that CTR1 is a direct target of MBZ in Arabidopsis.
314 To further test the hypothesis that MBZ acts upon CTR1, we utilized a readout directly
315 downstream of CTR1. Previous studies had shown that functional CTR1 phosphorylates
316 the carboxyl end of EIN2, leading to its degradation (Ju et al., 2012; Qiao et al., 2012a;
317 Wen et al., 2012). When ethylene inactivates CTR1, EIN2-CEND is stabilized and moves
318 into the nucleus to activate downstream ethylene responses. We therefore tested if MBZ
319 treatment mimicked ethylene for inducing EIN2 accumulation in the nucleus using 3-day-
320 old etiolated seedlings of two independent transgenic *EIN2-GFP* reporter lines in which
321 the GFP was fused to EIN2's C-terminus (*pEIN2::EIN2-GFP* in the *ein2-5* background (Fu
322 et al., 2021)). As expected, treatment with ACC quickly increased the nuclear
323 accumulation of EIN2-GFP in root cells (Figure 7A, B). Consistent with our hypothesis
324 that MBZ acted on CTR1, MBZ also significantly increased accumulation of EIN2-GFP in
325 the nucleus (Figure 7A, B). Taken together, our data support a model in which MBZ is a
326 small molecular inhibitor of the CTR1 kinase activity and thereby triggers the ethylene
327 signaling pathway by permitting C-terminal of EIN2 translocation into the nucleus, which
328 in turn triggers ethylene downstream responses (Figure 7C, D).
329

330 **DISCUSSION**

331 Our chemical genetic screen led to the identification of MBZ as a potent inhibitor of the
332 kinase activity of CTR1, which is a negative modulator of the ethylene signaling pathway
333 (Figure 7C). MBZ therefore is an activator of ethylene signaling, and to our knowledge
334 the first small molecule that acts downstream of ethylene receptors and that directly
335 activates ethylene signaling. In previous studies, ethylene gas and ACC have been used
336 to activate the ethylene signaling pathway. However, there were some disadvantages to
337 use these approaches. In the case of treatment with ethylene gas, it is difficult to maintain
338 a continuous treatment over longer periods of time due to the technical challenges for
339 constantly maintaining the required ethylene concentrations. Because its controlled
340 application is technically less challenging, ACC has been used more widely to study the
341 role of ethylene. However, ACC was recently found to be a signaling molecule which can
342 act independently of the ethylene pathway (Mou et al., 2020). Moreover, the necessity for

343 enzymatic ACC conversion to ethylene in plants might be limiting in different tissues or
344 conditions. While MBZ is not a perfect ethylene substitute and might have unspecific
345 effects beyond activating ethylene signaling, as a direct activator of the ethylene signaling
346 pathway, it promises to be a useful tool for the field. Such tools have been lacking so far
347 despite several attempts that have been made to identify small molecular regulators of
348 ethylene signaling. Neither approaches targeting ethylene biogenesis and perception, nor
349 approaches targeting downstream auxin biosynthesis had yielded in molecules acting on
350 ethylene signaling (He et al., 2011; Li et al., 2017; Sun et al., 2017; Zhu et al., 2019).
351
352 Because CTR1 contains the critical MBZ binding residues that had been elucidated in the
353 human MBZ target *hs*MPK14, and because of the profound genetic evidence for CTR1,
354 it is somewhat unlikely that other components in the ethylene pathway such as the E3
355 ligases ETP1/2 and EBF1/2, which negatively regulate EIN2 and EIN3 respectively (Guo
356 and Ecker, 2003; Qiao et al., 2012b), are targets of MBZ. Another signaling pathway that
357 impinges on ethylene signaling is the glucose-activated TOR signaling pathway, which
358 had recently been shown to regulate EIN2 activity through phosphorylation (Fu et al.,
359 2021). However, the TOR kinase does not contain any of the 4 key residues known for
360 MBZ binding. Moreover, unlike MBZ, none of the inhibitors of TOR, including Rap, Torin2,
361 and AMA, did induce the ethylene induced triple response phenotype (Fu et al., 2021). In
362 addition, *ein2-5* and *ein3 eil1* mutants displayed a shorter hypocotyl when the Glu-TOR-
363 EIN2 pathway was inhibited (Fu et al Nature 2021, Figure 1b), but these mutants did not
364 respond to MBZ treatment (Figure S3D, E). Altogether, it is most likely that the observed
365 response of MBZ on the ethylene signaling is exerted via its binding to CTR1.
366
367 While most of the effects of MBZ are related to its activation of ethylene signaling, our
368 RNA profiling indicated additional effects of MBZ. Consistently, treatment with high
369 concentration of MBZ or long-term treatment with it led to strongly inhibited plant growth
370 and development, including a disrupted root apical meristem and morphological changes
371 of leaves. These phenotypes have not been observed upon ethylene treatment (Figure
372 S5A, B), raising the possibility that MBZ may have other targets in plants. MAPK4 has the
373 highest amino acid sequence similarity to the human MBZ target *hs*MAPK14 (Table S1).

374 Compared to CTR1, the effect of MBZ on MAPK4 kinase activity was much less
375 pronounced (Figure 6C), consistent with the lack of conservation of key amino acids
376 relevant for MBZ binding (Figure S4C). Although MBZ couldn't inhibit the kinase activity
377 of MAPK4 as strongly as that of CTR1-KD, a decrease of the weak MAPK4
378 autophosphorylation band might indicate that MBZ treatment can disrupt MAPK4
379 autophosphorylation (Figure 6C). This raises the possibility that MBZ might alter
380 autophosphorylation of MAPK4 and probably other CTR1-like kinases, based on the
381 sequence conservation of the four critical residues (Figure 6A, Figure S4B). This might
382 explain the additional effects of MBZ. Additionally, there are a number of CTR1 paralogs
383 in Arabidopsis. This includes the kinases encoded by AT4G24480, AT1G08720,
384 At1g18160, AT1G67920, and AT5G11850. These kinases contain all four critical amino
385 acids, raising the possibility that MBZ may also bind to these paralogs. Another
386 explanation for the observed effects of MBZ that go beyond observed ethylene effects,
387 might be that continuous activation of ethylene signaling via CTR1 might have more
388 complicated or compounded effects than are elicited by external ethylene or ACC
389 treatment (Figure S5C). Support for this comes from the *ctr1-1* mutant, which is dwarfed
390 and shows aberration in leaf shape and thereby displays much stronger phenotypes than
391 elicited with ACC or ethylene treatment (Kieber et al., 1993) (Figure 5B, D, Figure S5C).
392 While MBZ's predominant effect on ethylene signaling via CTR1 is strongly supported by
393 our study, further studies will be needed to elucidate the details of MBZ specificity.
394
395 One of the most intriguing effects of MBZ on the plant is its potent ability to change GSA.
396 This suggests that ethylene signaling is involved in the regulation of the gravitropic
397 setpoint angle in lateral roots. While important regulatory roles for GSA are known for
398 auxin and cytokinin, and there can be complex interplays between auxin, cytokinin and
399 ethylene, the induction of the ethylene signaling pathway clearly dominated responses in
400 lateral roots after they were treated with MBZ (Figure 2). This activation of the ethylene
401 responses occurred before angles of lateral roots were changing and was maintained
402 throughout the timescale at which GSA was changed by the MBZ treatment, which
403 occurred after 1-4 hours of MBZ treatment (Figure 1E, F, Figure 2, Figure S2I). In our
404 study, we found that MBZ didn't induce ethylene biosynthesis (Figure 4A). ACC treatment

405 had a weak but distinct effect on root angle and displayed concentration-dependent
406 effects when applying a large range of concentrations (Figure S5C). Strong direct
407 evidence for the impact of ethylene signaling in regulating lateral root set point angle is
408 provided by the RSA phenotype of the *ctr1-1* mutant. In *ctr1-1*, ethylene signaling is
409 constitutively activated and leads to an increased lateral root angle (Figure 5D, E).
410 Conversely, we observed that the ethylene insensitive *ein2-5* mutant displays steeper
411 lateral roots (Figure 5F, G). Overall, this exposes a yet unknown role of ethylene signaling
412 in the regulation of lateral root set point angle. One reason why the role of ethylene in the
413 regulation of lateral root angles hasn't been recognized so far might be that it reduces
414 lateral root formation by itself (Negi et al., 2008) making the study of lateral root angles
415 more difficult. Our study strongly suggests that it will be worthwhile to explore the role of
416 ethylene and its interaction with auxin and cytokinin in root gravitropism and RSA.
417 Moreover, MBZ might also be used as a versatile tool for exploring the molecular
418 mechanisms of root gravitropism and lateral root set point angles since as a small
419 molecule, and due to its reversible mode of action, it can be easily applied to elicit
420 controlled changes of lateral root angles. It might also be useful to reveal the mechanisms
421 underlying GSA regulation by phytohormones and known GSA signals, such as the *LAZY*
422 family genes (Furutani and Morita, 2021). Finally, since ethylene signaling is a widely
423 conserved process in land plants, exploring the ability of MBZ or genetic perturbation of
424 the ethylene pathway to change RSA in crop species might be highly worthwhile for RSA
425 engineering.
426

427 **Acknowledgements**

428 The research was supported by start-up funds from the Salk Institute for Biological
429 Studies and funds from the Harnessing Plants Initiative to WB, a Salk Women & Science
430 Special Award and a Pioneer Fund Postdoctoral Scholar Award to WH. We are grateful
431 to Dr. Glenn R. Hicks and Dr. Natasha Raikhel for sharing the SP2000 small molecule
432 library. We thank Dr. Cris Argueso, Dr. Dolf Weijers, and Dr. Liwen Fu for sharing seeds.
433 We also thank Dr. Joseph R. Ecker and Dr. Joanne Chory for critical discussions. We
434 thank the Next Generation Sequencing Core of Salk institute for NGS Library preparation

& sequencing. We also thank Matthieu Platre, Nicole Gibbs, Anna Malolepszy, Björn Willige and Travis Lee for fruitful discussions and suggestions.

Author contributions

Wenrong He and Wolfgang Busch conceived the project and the experiments. Wenrong He performed the SP2000 library screen and analysis with help from Yingnan Hou. Wenrong He performed the phenotyping, qPCR, alignment, docking, protein purification, kinase activity assay. Wenrong He conducted the microscopy and mRNA-seq on primary roots with help from Kaizhen Zhong. Hai An Truong performed the time lapse reporter analysis using spinning disk microscopy, as well as the whole root system and lateral root RNA-seq experiments. Ling Zhang conducted the mRNA-seq analysis and the statistical analysis. Wenrong He conducted heatmap analysis of mRNA-seq. Wenrong He and Ling Zhang conducted Gene ontology analysis. Min Cao provided the protocol and suggestions for kinase activity assay. Neal Arakawa performed the GC test. Yao Xiao performed the FPLC. Wenrong He and Wolfgang Busch wrote the manuscript with input from all authors. Wolfgang Busch provided materials, funding, supervision, guidance and advice on the project, the experiments, and the analysis of the results.

Declaration of Interests

W.B. is a co-founder of Cquesta, a company that works on crop root growth and carbon sequestration.

FIGURE LEGENDS

Figure1. MBZ treatment perturbs root system architecture (RSA).

(A) 14-day-old Arabidopsis seedlings of grown on DMSO and MBZ (1 μM) plates.

(B) Quantification of GSA in (A). 15 LRs per seedling on DMSO plates, 12 LRs per seedling on MBZ plates, and 6 seedlings for each condition were used. Unpaired, two-tailed Student's t-tests was used for statistical analysis. **** $p < 0.0001$.

(C) 7-day-old seedlings on DMSO and MBZ (1 μM) plates.

466 (D) Quantification of primary root length (cm) in (B). 15-20 seedlings for each treatment
467 were used. **** $p < 0.0001$.
468 (E) 14-day-old (upper panel) Arabidopsis seedlings on DMSO plates were transferred to
469 MBZ (1 μM) plates, and 19-day-old (bottom panel) seedlings on MBZ (1 μM) plates were
470 transferred to DMSO plates, followed by continuous scanning for 24 h.
471 (F) Changes of lateral root angle after plate transfer from DMSO to MBZ (red and yellow
472 lines) or MBZ to DMSO (blue, purple lines) compared to timepoint 0.
473 (Scale bar: A, C, G, 1 cm; E, 5 mm.). Boxplots: Whiskers: min/max values; hinges: 25th
474 to 75th percentile; mid-line: median.
475
476 **Figure 2. MBZ treatment regulates the ethylene pathway**.
477 (A) Gene ontology (GO) analysis upregulated genes (abs(log2) fold change > 1) from
478 DEGs upon MBZ treatment in roots of 14-day-old Arabidopsis seedlings.
479 (B) Heatmap of DEGs involved in the ethylene pathway, which were detected to be
480 differentially expressed upon MBZ treatment in the RNA-seq analysis. The left 4 columns
481 of DMSO are data from 4 replicates of samples from DMSO (Mock) plates. The right 4
482 columns of MBZ are data from 4 replicates of samples from MBZ treatment plates. The
483 heatmap was made online by heatmapper (http://heatmapper.ca/expression/), The
484 cluster method is complete linkage. Color bar indicates the relative expression level.
485 (C-E) Venn diagrams showing differentially expressed genes in 3 h MBZ treatment and 3
486 h ACC treatment. All genes (FDR < 0.05; abs(log2) fold change > 1) (C), upregulated
487 genes (FDR < 0.05; log2 fold change > 1) (D), downregulated genes (log2 fold change <
488 -1) (E).
489 (F) Dot plots showing the most enriched GO terms with KS p-value < 0.05 from DEGs
490 upon MBZ treatment in lateral root tips of 14-day-old seedlings.
491 **(**G-I**)** Representative images of lateral root tips of two-week-old plants in response to
492 negative control, positive control and MBZ treatment using ethylene (*EIN3-GFP*)(G),
493 auxin (*DR5v2-GFP*)(H), and cytokinin (*TCSn-GFP*)(I) reporter lines at 0 and 60 minutes
494 of treatment.
495 **(**J**)** Relative fluorescent intensity of *EIN3-GFP* lateral root tips treated over a course of 4
496 h with DMSO, MBZ, and ACC.

497 **(K)** Relative fluorescent intensity of *DR5v2-GFP* lateral root tips treated over a course of
498 4 h with DMSO, MBZ, and IAA.
499 **(L)** Relative fluorescent intensity of *TCSn-GFP* lateral root tips treated over a course of 4
500 h with DMSO, MBZ, and tZ. 6 lateral roots for each treatment were used. Unpaired, two-
501 tailed Student's t-tests were used to compare the data of MBZ or the corresponding
502 positive controls to DMSO at each timepoint. *: $p<0.05$; **: $p<0.01$; ***: $p<0.001$.
503
504 **Figure 3. MBZ induces ethylene responses and mimics ACC treatment**.
505 (A) 4-day-old etiolated seedlings grown on MS, 10 μM ACC, DMSO, 10 μM MBZ plates.
506 20 Col-0 seedlings for each treatment were observed and 2 representative seedlings for
507 each treatment are shown in the panel.
508 (B-C) Quantification of hypocotyl length (B) and primary root length (C) of seedlings in
509 (A). 20 Col-0 seedlings for each treatment were used. **** $p < 0.0001$.
510 (D) Images of median longitudinal optical sections of primary root meristem and mature
511 zone stained with propidium iodide (PI) of 4-day-old etiolated Col-0 on DMSO, 2.5 μM
512 MBZ, and 10 μM ACC plates, 6-10 seedlings were observed for each treatment.
513 (E-F) Meristem length (E) and mature cell size (F) of seedlings in (D). 6-10 seedlings for
514 each treatment were used. Different letters label significant different values ($p<0.0001$).
515 One-way ANOVA and *post hoc* Tukey testing were used for statistical analysis in (E) and
516 (F). (Scale bar: **A**, 5 mm; **D**, 100 μm.). Boxplots: Whiskers: min/max values; hinges: 25th
517 to 75th percentile; mid-line: median.
518
519 **Figure 4. MBZ acts downstream of ethylene biosynthesis**.
520 (A) Quantification of ethylene production by GC-MS of 4-day-old etiolated seedlings of
521 Col-0 in vials with DMSO, 10 μM MBZ, and 10 μM ACC medium. 100 seedlings for every
522 vial, 4 biological replicates for each treatment, ND: not detectable.
523 (B) 6-day-old seedlings of Col-0, *etr1-1*, and *etr1-3* grown on DMSO and 1.2 μM MBZ
524 plates. 20 seedlings were observed.
525 (C) Quantification of root length in (A). 20 seedlings were countified.
526 (D) 16-day-old seedlings of Col-0 and *etr1-1* grown on DMSO and 1.2 μM MBZ plates. 20
527 seedlings were observed.

528 (E) Quantification of GSA in (C). 20 seedlings were countified.
529 One-way ANOVA and *post hoc* Tukey testing were used for statistical analysis in b and
530 d. Different letters label significant different values ($p<0.0001$). (Scale bar: **B**, **D**, 1 cm.)
531 Boxplots: Whiskers: min/max values; hinges: 25th to 75th percentile; mid-line: median.
532
533 **Figure 5. MBZ targets the ethylene signaling pathway**.
534 (A) Diagram of ethylene signaling pathway.
535 (B) 7-day-old seedlings of Col-0, *ctr1-1*, and *ein2-5* grown on DMSO and 1.2 μM MBZ
536 plates.
537 (C) Quantification of primary root length of seedlings in (B) 15-20 seedlings were
538 quantified. Similar results were obtained from three biological replicates of the
539 experiment.
540 (D) 19-day-old seedlings of Col-0 and *ctr1-1* grown on DMSO and 1.2 μM MBZ plates.
541 (E) Quantification of GSA of seedlings in (D). 10 seedlings were quantified. Similar results
542 were obtained from three biological replicates of the experiment.
543 (F) 16-day-old seedlings of Col-0 and *ein2-5*, *ein3 eil1* grown on DMSO and 1.2 μM MBZ
544 plates.
545 (G) Quantification of GSA of seedlings in (F). *dm* stands for *ein3 eil1* double mutants.
546 One-way ANOVA and *post hoc* Tukey testing were used for statistical analysis in **C**, **E**,
547 and **G**. Different letters label significant different values ($p<0.0001$). (Scale bar: **B**, **D**, **F**,
548 1 cm.). Boxplots: Whiskers: min/max values; hinges: 25th to 75th percentile; mid-line:
549 median.
550
551 **Figure 6. MBZ inhibits CTR1 kinase activity**.
552 (A) Sequence alignment of *hs*MAPK14 and CTR1-KD in Arabidopsis around 4 core amino
553 acids (Highlighted by blue and pink frames) for MBZ binding.
554 (B) Molecular modeling of the interaction between MBZ (coppery) and CTR1-KD (silvery).
555 In the left panel, the key residues that contribute to the binding with CTR1-KD were
556 highlighted. The right panel showed the surface (gray) of the catalytic pocket of CTR1-
557 KD.

558 (C) Western blot using Recombinant Anti-Thiophosphate ester antibody under different
559 concentration of MBZ treatment. Left panel: CTR1-KD; Right panel: MAPK4. MBP is the
560 substrate in both panels, MBZ concentration is 0, 10, and 100 μM as labeled in different
561 reactions, [ATPγS]CTR1-KD: ATPγS binding CTR1-KD, [ATPγS]MAPK4: ATPγS binding
562 MAPK4, MBP that obtained ATPγS from CTR1-KD or MAPK4, which is labeled as
563 [ATPγS]MBP. Note: ATPγS: Adenosine 5'-(3-thiotriphosphate) tetralithium salt (Sigma,
564 Cat# A1388)
565 (D) Coomassie blue staining of the gel shown in (C). CTR1: ~100 ng, MAPK4: ~1 μg.
566 Myelin Basic Protein (MBP, a common kinase substrate, Sigma Cat. M1891): 2 μg,
567 ATPγS: 1 mM. MBZ: 0, 10, or 100 μM. Arrows label the position of these bands on the
568 gel.
569
570 **Figure 7. MBZ activates ethylene signaling**.
571 (A) Different patterns of nuclear accumulation of *EIN2-GFP* in root cells. 3-day-old
572 etiolated seedlings treated with Mock, ACC (100 μM), or MBZ (10 μM) for 3 hours. Arrows
573 indicate nuclei. (Scale bar: 20 μm).
574 (B) Quantification of Relative GFP fluorescent intensity between the nucleus and cytosol
575 of *EIN2-GFP* in **A**. Boxplots: Whiskers: min/max values; hinges: 25th to 75th percentile;
576 mid-line: median. One-way ANOVA and *post hoc* Tukey testing were used for statistical
577 analysis.
578 (C,D) Model for MBZ activation of ethylene signaling. (C) Ethylene suppresses CTR1
579 activity to promote EIN2C translocation and activates ethylene signaling. (D) MBZ inhibits
580 CTR1 activity by binding to its kinase domain and promotes EIN2C translocation to
581 activate the ethylene signaling.
582 Note: EIN2C: C-terminal of EIN2; ATP: Adenosine triphosphate; ADP: adenosine
583 diphosphate; C2H4: ethylene; P: Phosphate group. The CTR1 with orange color means
584 active CTR1 proteins and the CTR1 with gray color means inactive CTR1.
585
586 **Figure S1. MBZ treatment affects root growth and development**.
587 (A) Chemical structure of MBZ.

588 (B-C) Root hair phenotype of 7-day-old seedlings on DMSO and 1 μM MBZ plates
589 recorded by a scanner (B) or a microscope (C). 20 seedlings were observed on left panel
590 and 10 seedlings were observed on right panel. (Scale bar: **B**, 13 mm; **C**, 1000μm)
591
592 **Figure S2. Analysis of differentially expressed genes (DEGs) upon MBZ treatment.**
593 (A-C) Venn diagrams showing differentially expressed genes in 4 h MBZ treatment in
594 roots of 14-day-old green seedlings and published 4 h ethylene treatment in 3-day-old
595 etiolated seedlings. All genes (FDR<0.05; abs(log2) fold change > 1) (A), upregulated
596 genes (FDR<0.05; log2 fold change > 1) (B), downregulated genes (FDR<0.05; log2 fold
597 change < -1) (C).
598 (D) Gene ontology (GO) analysis of upregulated genes (FDR<0.05; log2 fold change > 1)
599 from DEGs upon MBZ treatment.
600
601 **Figure S3. Etiolated seedling phenotypes in mutants of the ethylene pathway.**
602 (A) 4-day-old etiolated seedlings of Col-0 and *etr1-3* grown on DMSO, 2.5 μM MBZ, and
603 10 μM ACC plates.
604 (B-C) Quantification of hypocotyl length (B) and root length (C) of seedlings in (A). 20
605 seedlings were quantified.
606 (D) 4-day-old etiolated seedlings of Col-0, *ctr1-1, ein2-5*, and *ein3 eil1* grown on DMSO,
607 2.5 μM MBZ, and 10 μM ACC plates.
608 (E-F) Quantification of hypocotyl length (E) and root length (F) of seedlings in **D**. 20
609 seedlings were quantified. Statistical analysis in **B, C** and **E, F** were done using unpaired,
610 two-tailed Student's t-tests. P-values are indicated in the figure. (Scale bar: **A, D**, 1 cm).
611 Whiskers: min/max values; hinges: 25th to 75th percentile; mid-line: median.
612
613 **Figure S4. Alignment of CTR1-KD in Arabidopsis and MAPK14 in human**.
614 (A) The structure alignment of *hs*MAPK14 (coppery) and CTR1-KD (celeste).
615 (B) The protein binding sites in *hs*MAPK14 (coppery) and CTR1-KD (periwinkle) with
616 highlighted key residues.
617 (C) Sequence alignment of kinase domains. Key residues in MAPK14_human and CTR1-
618 KD in Arabidopsis are indicated by red boxes.

619 (D) Phylogenetic analysis of kinases aligned in (C).

620

621 **Figure S5. High concentrations or long-term treatment of MBZ induce phenotypes**
622 **that go beyond ethylene induced effects**.
623 (A) Confocal microscopy images of a root meristem of 4-day-old etiolated WT seedling
624 grown on 10 μM MBZ plate.
625 (B) 38-day-old Col-0 plants grown on DMSO and 1.2 μM MBZ plates.
626 (C)14-day-old seedlings of Col-0 grown on increasing concentrations MBZ and ACC (0.1,
627 0.2, 0.4, 1, 2, 4, 10 μM) 20 seedlings were observed. Similar results were obtained from
628 three biological replicates of the experiment. (Scale bar: **A**, 100 μm, **B**, **C**, 1 cm)

629

630 **Table S1. The list of blast hits in Arabidopsis using the MAPK14_human sequence**
631 **as BLASTP**.

632

633 **KEY RESOURCES TABLE**

REAGENT or RESOURCE	SOURCE	IDENTIFIER
Antibodies		
Recombinant Anti-Thiophosphate ester antibody	Abcam	Cat# Ab92570
Chemicals, Peptides, and Recombinant Proteins		
SP 2000 small molecule library	(He et al., 2011)	Gift from UC Riverside
Mebendazole	ACROS	Cat# 101720050
DMSO	Alfa Aesar	Cat# 36480
ACC	Sigma	Cat# A3903
IAA	Alfa Aesar	Cat# A10556
Maxima™ H Minus cDNA Synthesis Master Mix, with dsDNase	Thermo Scientific	Cat# M1682
Luna® Universal qPCR Master Mix	NEB	Cat# M3003L
MBP	Sigma	Cat# M1891
ATP γ S	Sigma	Cat# A1388
PNBM	CAYMANCHEMICAL	Cat# 21456-1
Experimental Models: Organisms/Strains		
Arabidopsis: *etr1-1*	ABRC	CS237
Arabidopsis: *etr1-3*	ABRC	CS3070
Arabidopsis: *ctr1-1*	(Kieber et al., 1993)	N/A
Arabidopsis: *ein2-5*	(Alonso et al., 1999)	N/A
Arabidopsis: *ein3-1eil1-1*	(Alonso et al., 2003)	N/A
Arabidopsis: *ein3 eil1 35S: EIN3-GFP*	(He et al., 2011)	N/A
Arabidopsis: *UBQ10p:TUB6-GFP*	(Nakamura et al., 2004)	N/A
Arabidopsis: *35S:DR5v2:3xGFP-NLS*	(Liao et al., 2015b)	Weijers lab
Arabidopsis: *TCSn-GFP*	(Zürcher et al. 2013)	Argueso lab
Arabidopsis: *EIN2-GFP in ein2-5*	(Fu et al., 2021)	Fu Lab
Oligonucleotides		
ERF1Q-PCRF: ATTCTTTCTCATCCTCTTCTTCT	This paper	N/A
ERF1Q-PCRR: CGAATCTCTTATCTCCGCCG	This paper	N/A
AtACTIN2F: TTGACTACGAGCAGGAGATGG	This paper	N/A
AtACTIN2R: ACAAACGAGGGCTGGAACAAG	This paper	N/A
UBQ10F: CGTCAAGGCCAAGATCCAAG	This paper	N/A
UBQ10F: CAGCAAGAGTTCTGCCATCC	This paper	N/A
EcoR1-CTR1-atg-540-F: GGGGAATTCATGGATGGTGATGATATGGACATCCCG	This paper	N/A
sal-CTR1-821-R: GGGGTCGACTTACAAATCCGAGCGGTTGGGCGGA	This paper	N/A
EcoR1-MPK4-F: GGGGAATTCATGTCGGCGGAGAGTTGTTTC	This paper	N/A

sal-MPK4-R: GGGGTCGACTCACACTGAGTCTTGAGGATTGAAC	This paper	N/A
Recombinant DNA		
pET28a-CTR1-KD	This paper	N/A
pET28a-MAPK4	This paper	N/A
Commercial Kits		
Spectrum™ Plant Total RNA Kit	Sigma	Cat# STRN250
Software and Algorithms		
Fiji	(Schindelin et al., 2012)	(http://fiji.sc/Fiji).
GraphPad Prism	GraphPad	Version 9.3.1
Heatmapper	(Babicki et al., 2016)	(http://heatmapper.ca/)
AutoDock Vina	(Trott and Olson, 2010)	(https://vina.scripps.edu/)
Chimera	(Pettersen et al., 2004)	(https://www.cgl.ucsf.edu/chimera/)
Other		

CONTACT FOR REAGENT AND RESOURCE SHARING

Further information and requests for resources and reagents should be directed to and will be fulfilled by the Lead Contact, Wolfgang Busch (wbusch@salk.edu).

EXPERIMENTAL MODEL AND SUBJECT DETAILS

Arabidopsis thaliana

Arabidopsis mutants and transgenic lines used in this study are in the Col-0 background if not mentioned otherwise. *etr1-1* (CS237) and *etr1-3* (CS3070) were ordered from ABRC, *ctr1-1* (Kieber et al., 1993) *ein2-5* (Alonso et al., 1999), *ein3-1 eil1-1*(Alonso et al., 2003), *ein3 eil1 35S: EIN3-GFP* (He et al., 2011), and *UBQ10p:TUB6-GFP* (Nakamura et al., 2004) were lab stock. *35S:DR5v2:3xGFP-NLS* (Liao et al., 2015b) was gift from Weijers lab (Col-Ultrecht background). *TCSn-GFP* (Zurcher et al., 2013) was a gift from Argueso

646 lab. *EIN2-GFP* (Fu et al., 2021) in *ein2-5* was a gift from Fu lab. Plants were sown on half
647 Murashige and Skoog (MS) medium with 1% (wt/vol) sugar, 0.1 % (wt/vol) MES (pH 5.75),
648 containing 1% (wt/vol) agar supplemented with different chemicals as descripted in the
649 article. Following a 3-day stratification in the cold room (4~10°C), for green seedling assay,
650 plants were grown on vertical plates in a walk-in growth chamber with long day conditions
651 (16/8 h) at 21°C, 50 μM light intensity, 60% humidity. During nighttime, temperature was
652 decreased to 15°C. For etiolated seedling assay, the plates were placed in light for 4 h
653 and then germinated in the dark for 3 day in the growth chamber at 22 °C.
654 Plants were grown on vertical plates in a walk-in growth chamber with long day conditions
655 (16/8 h) at 21°C, 50 μM light intensity, 60% humidity. During nighttime, temperature was
656 decreased to 15°C.

657 **Accession Numbers**

658 Sequence data from this article can be found in the Arabidopsis Genome Initiative or
659 GenBank/EMBL databases or Uniprot databases under the following accession numbers:
660 *ERF1* (AT3G23240), *ETR1* (AT1G66340), *CTR1* (AT5g03730), *EIN2* (AT5G03280), *EIN3*
661 (AT3g20770), *EIL1* (AT2G27050), *MAPK4* (AT4G01370), and *hsMAPK14* (HGNC:6876).
662 Accession numbers of protein and chemicals structures used in the molecular modeling
663 in Figure 6 are as follows: CTR1 (PDB: 3PPZ), MAPK14 (PDB: 6SFO) and MBZ
664 (CHEMBL685).

665 **METHOD DETAILS**

666 **Small Molecule Library and Screen Information**

667 The SP2000 small molecule library was received from the University of California,
668 Riverside. The library was first screened at a concentration of 50 ~ 100 μM in 200 μL of
669 liquid MS media using wild type Arabidopsis. After being grown in the liquid media with
670 small molecules for 7 days, seedlings were transferred to vertical plates to grow for
671 another 2 days. The root phenotypes were acquired by CCD flatbed scanners. After
672 candidates were picked, a second round of screen was performed by growing Col-0
673 seedlings on vertical plates with gradient concentration of candidate small molecules,
674 from 1 μM to 100 μM, for 14 days to confirm the phenotype and optimal concentration.
675

676 **Cloning and constructs**

677 To produce recombinant CTR1 kinase domain (CTR1-KD) and MAPK4 proteins in *E. coli*,
678 the coding sequences of 540-821 aa of CTR1and full length MAPK4 were PCR amplified
679 from cDNA of Arabidopsis Col-0, using gene-specific primers (listed in KEY
680 RESOURCES TABLE). The PCR products were inserted into pET28a using restriction
681 digestion and ligation with EcoR 1 and Sal 1 (NEB) sites.
682
683 **Chemical Solutions**
684 The stock solutions for preparing media for the plant experiments were Mebendazole (10
685 mM) in DMSO, ACC (10 mM) in dH2O, IAA (1 mM) in ethanol.
686
687 **Root phenotyping**
688 Images of root phenotypes on plates were acquired with CCD flatbed scanners (EPSON).
689 Root lengths and lateral root angles were measured using Fiji (http://fiji.sc/Fiji).
690
691 **Lateral root angle measurement**
692 The lateral root angle of individual LRs was measured according to (Rosquete et al.,
693 2013b) using Fiji. LRs after stage III from each seedling were measured according to
694 (Rosquete et al., 2013b; Waidmann et al., 2019a) .
695
696 **Time lapse of lateral root angle phenotyping**
697 14-day-old seedlings on DMSO plate or 19 d old seedling on mebendazole plate were
698 transferred to DMSO or 1 μM mebendazole plates as described (Figure 1E). Root
699 phenotype images were acquired by CCD vertical scanners (EPSON) every 10 mins over
700 a period of 24 hours using the tool described(Ogura et al., 2022). Root length and lateral
701 root angles were measured using Fiji (http://fiji.sc/Fiji).
702
703 **mRNA-seq**
704 **A. Tissue preparation**
705 Roots or lateral root tips of 14-day-old Col-0 seedlings with different treatment were
706 collected for the mRNA-seq analysis. In detail:
707 **a. Roots**

708 Sterilized seeds of Col-0 on ½ MS media were planted on a mesh in one row (~more than
709 30 seeds/plate). 5 plates were used for one treatment condition for every replicate, and 4
710 replicates were used for every treatment. After 14 days of vertical growth in the chamber,
711 liquid media of ½ MS with DMSO (0.1 %, v/v), 10 μM MBZ, and 10 μM ACC (to be
712 consistent, we also added the same concentration of DMSO (0.1 %, v/v) in the ACC
713 treatment plates) were prepared. 10 mL liquid treatment medium was used on each plate.
714 The mesh with seedlings from ½ MS plates was transferred the respective liquid
715 treatment plates and kept in growth chamber. After 4 hours for the mRNA-seq of MBZ
716 treatment and 3 hours for the mRNA-seq of MBZ and ACC treatment, roots were collected
717 using scalpel and tweezers. Excess liquid on the roots was removed using a paper towel.
718 Root samples were flash-frozen in liquid nitrogen and then stored at -80 freezer before
719 RNA extraction.
720 For RNA extraction, root tissues were ground in liquid nitrogen and RNA was extracted
721 using Quick-RNA Kits (Zymo research). RNA libraries were prepared for sequencing
722 using standard Illumina protocols at the Salk Next Generation Sequencing Core (NGS).
723 Note: We used liquid media for DMSO, MBZ, and ACC treatment in the mRNA-seq of
724 roots to detect transient gene regulation as these chemicals in liquid media can be
725 sufficiently and equally absorbed into lateral roots and reduce time for sample collection.
726 **b. Lateral root tips**
727 Sterilized seeds were grown for 14 days on ½ MS medium. The seedlings were then
728 transferred to freshly prepared DMSO or 1μM MBZ plates for 4 hours on 15 plates (5
729 plants/plate) for each treatment. 4 biological replications were performed. A stereo
730 microscope (Leica) was used to dissect the meristem area of lateral root tips in order to
731 collect the lateral root tips. The cut lateral root tips were quickly placed into 1.5
732 microcentrifuge tubes that floated on liquid nitrogen. This process was repeated until
733 approximately 400 root tips were collected per sample.
734 The NucleoSpin RNA extraction kit (Macherey-Nagel) was used to extract total RNA. The
735 concentration and integrity of extracted RNA were determined using Qubit and
736 TapeStation 2200 before being sent to Salk Next Generation Sequencing Core (NGS) for
737 library preparation and sequencing.
738

739 **B. Data analysis**

740 **a. Read alignment**

741 The TAIR10 genome file and annotation file were obtained from the Arabidopsis
742 Information resource web site (http://www.arabidopsis.org)(Berardini et al., 2015). The An
743 aligner, called the Splice Transcripts Alignments to Reference (STAR) version 2.7.0a
744 (Dobin et al., 2013), was used to align short reads in the FASTQ files.

745 **b. Differential expression analysis**

746 Differential expression of genes between treatments and control was determined using
747 the R package, *edgeR* (version 3.36.0)(Robinson et al., 2010). The *CPM* (counts per
748 million) function from *edgeR* was used to normalize the counts and differentially
749 expressed genes (DEGs) were identified using *glmLRT* function from edgeR. A false
750 discovery rate (FDR < 0.05) and |log2FC| > 1 were used as the criterial values for
751 identification of up-regulated and down-regulated DEGs.

752

753 **GO analysis**

754 Gene Ontology analysis of up-regulated DEGs (FDR < 0.05) and |log2FC| > 1 by MBZ
755 treatment in roots of 14-day-old Arabidopsis seedlings was performed with PANTHER
756 Overrepresentation Test (Released 20230705). The Annotation Version used GO
757 Ontology database (DOI: 10.5281/zenodo.7942786 (Released 20230510)). Enriched
758 genes (Bonferroni-corrected for P < 0.05) for biological processes were listed (Figure 2A).
759 We used R package topGO (version 2.42.0)(Alexa et al., 2006) with the weight01
760 algorithm and the mappings from the "org.At.tair.db" R package to perform functional
761 enrichment analysis of DEGs by MBZ treatment in roots and lateral root tips of 14-day-
762 old Arabidopsis seedlings. We carried out KS test for statistical comparison. Then we
763 used "ggplot2" package in R to plot 30 most enriched gene ontology terms (GO) which
764 were ordered by Kolmogorov-Smirnov p-values for biological processes (Figure 2F, S2D).

765

766 **Measurement of ethylene production.**

767 100 seeds of Col-0 were planted and sealed in a screw-top 20 mL vial containing 10 mL
768 ½ MS medium supplemented with DMSO (control), 10 μM mebendazole, and 10 μM ACC
769 treatments (4 replicates). These vials were incubated at 22 °C for 3 days under dark

770 environment. 500-1000 μL sample of the headspace gas was sampled with an
771 autosampler (TriPlus RSH, Thermo Scientific) and injected into a gas chromatograph
772 (Trace 1310 GC, Thermo Scientific) that was equipped with a HP-PLOTQ column (30 mm,
773 320 μm, 20 μm) and a mass spectrometer (TSQ8000 Evo MS, Thermo Scientific),
774 scanning from 25-27.5 m/z. Separations were carried out at 35°C using He as the carrier
775 gas. The area of the ethylene peak (RT: 4 min) was integrated using Thermo Xcalibur
776 Qual Browser. A calibration curve was generated by varying the injection volume (100
777 μL, 250 μL, 500 μL, and 1000 μL) of a 10 ppm ethylene standard (in nitrogen), and sample
778 results are expressed as concentrations calculated from linear regression of calibration
779 samples.
780
781 **qRT-PCR**
782 For measurement of marker genes of plant hormone pathways, 20 7d old seedlings of
783 Col-0 grown on ½ MS media were treated with DMSO or 10μM MBZ, dH2O or 10 μM
784 ACC for 2h, or 3, 6, 12h as described in the manuscript. Then whole roots were collected.
785 RNA extraction was performed using the Spectrum™ Plant Total RNA Kit (Sigma),
786 followed by cDNA synthesis using Maxima™ H Minus cDNA Synthesis Master Mix, with
787 dsDNase (Thermo Scientific). Quantitative PCR was performed with Luna® Universal
788 qPCR Master Mix (NEB). All procedures were carried out according to manufacturer
789 instructions. qRT-PCR primer information were listed in the KEY RESOURCES TABLE.
790
791 **Microscopy**
792 A Zeiss 710 confocal microscope with a 40x objective was used to detect propidium iodide
793 (PI) fluorescence in Figure 3F. A Keyence BZ-X810 microscope with a 20x objective was
794 used to detect bright field images and GFP fluorescence in Figure 3B, Figure S1B right
795 panel. A Leica TCS SP5 confocal microscope with 40x objective was used to detect GFP
796 fluorescence in Figure 7A.
797
798 **Accumulation of EIN2-GFP in root cells**
799 3-day-old etiolated seedlings of two independent transgenic *EIN2-GFP* reporter lines in
800 which the GFP was fused to EIN2's C-terminus (*pEIN2::EIN2-GFP* in the *ein2-5*

801 background (Fu et al., 2021)) were moved into different wells of 6-well plate with 5 mL
802 Mock (dH2O+ 5 μL DMSO), ACC (100 μM + 5 μL DMSO), or MBZ (10 μM). The plate
803 was then covered with tin foil to keep the dark environment for 3 hour. Then samples
804 were directly mounted on glass slides in their treatment liquid and observed under a Leica
805 SP5 microscope (Leica).
806
807 **Time lapse microscopy of reporter genes in lateral root tips**
808 To observe the response of ethylene (*EIN3-GFP*), auxin (*DR5v2-GFP*), and cytokinin
809 (*TCSn-GFP*) reporter lines to MBZ, 14-day-old seedlings grown on ½ MS media were
810 transferred to a Chambered Coverglass (Thermo Scientific) that was filled with treatment
811 medium. For chamber preparation, 6 mL of ½ MS medium (1 % agar) supplemented with
812 the different treatments (DMSO, 10 μM MBZ, 1 μM IAA, 50 μM ACC, and 10 μM tZ) was
813 filled to each chamber. After 20 minutes of medium solidification, the seedlings were
814 placed on the media surface and the lateral roots were adjusted to positions suitable for
815 imaging.
816 For imaging, a Zeiss CSU Spinning Disk Confocal Microscope equipped with laser 488
817 mm and a Yokogawa spinning disk scan head with EM-CCD camera were used to set up
818 the image acquisition every 20 minutes for a total of 4 hours. Three Z-stack positions were
819 automatically captured at each time point under 10X objective and Fiji was used to
820 quantify the average intensity of GFP fluorescence. For proper comparison at different
821 treatment conditions of each reporter lines, we normalized the average fluorescence data
822 as the percentages (or relative fluorescence intensity as text label). In detail, the first time
823 point of each treatment is set as 100% and the relative fluorescence intensity from the
824 second time point is calculated as the fold-change in percentages comparing the first time
825 point.
826
827 **Quantification of relative GFP fluorescent intensity between the nucleus and**
828 **cytosol**
829 The quantification of the microscopy localization data of *EIN2-GFP* in Figure 7B was done
830 according to (Fu et al., 2021) using LAS X (Leica Application Suite v. X3.1.1.15751) and
831 GraphPad Prism V9.5.1. In brief, the signal intensity of nucleus (Ni) and whole cell (Wi)

832 was quantified by LAS X (Mean value of nucleus * ROI Area of nucleus, mean value of
833 whole cell * ROI Area of whole cell), and then the signal intensity of cytosol (Ci) was
834 obtained by Wi minus Ni, and the area of cytosol (Sc) was obtained by the area of whole
835 cell (ROI Area of whole cell) minus the area of nucleus (ROI Area of nucleus). The mean
836 value of the signal intensity of cytosol (Mean Ci) equals Ci/Sc, and the relative GFP
837 fluorescent intensity between the nucleus and cytosol equals Mean value of nucleus/
838 Mean Ci.
839
840 **Computational Docking and Molecular Modeling**
841 The AutoDock Vina and Chimera software were used to dock mebendazole
842 (CHEMBL685) into crystal structure of CTR1 (PDB: 3PPZ) and MAPK14 (PDB: 6SFO).
843 Figures for those structures were visualized and generated by Chimera and Pymol.
844
845 **Protein purification**
846 The CTR1 Kinase domain (540 aa-821 aa) (CTR1-KD) and MAPK4 were cloned into a
847 pET28a. Proteins were expressed in Rosetta™ 2(DE3)pLysS Competent Cells. Cultures
848 were incubated at 37°C (OD 600:0.7 to 0.9) and induced by adding 0.4 mM
849 isopropylthioβ-D-galactoside (IPTG) at 20°C for 22 h, 200 rpm. Cells were harvested and
850 resuspended in lysis buffer (50 mM pH 7.5 Tris-HCl, 1mM EDTA, 100 mM NaCl, 20%
851 glycerol, EDTA-free protease inhibitor cocktail, 10 mM imidazole). followed by sonication
852 and centrifugation (13,000 × g × 20 min). The His-tagged proteins were first purified using
853 QIAGEN Ni-NTA Agarose. The elute from Ni-NTA was collected and further purified by
854 FPLC using superdex 200 Increase 10/300 column (Mayerhofer et al., 2011). The
855 fractions corresponding to single peak from FPLC were combined, and concentrated to a
856 desired volume. Protein purity was verified by Coomassie blue gel staining. Protein
857 concentration was measured by their absorbance at 280 nm.
858
859 ***In vitro* kinase assay with non-radioactive ATP-γ-S**
860 The *in vitro* kinase assay followed the previous published method (Allen et al., 2007). 100
861 ng purified recombinant CTR1-KD or 1 μg MPK4 was mixed with 2 μg Myelin Basic
862 Protein (MBP, a common kinase substrate, Sigma Cat. M1891) and 1 mM ATPγS in

863 kinase reaction buffer (10 mM HEPES pH 7.4, 150 mM NaCl, 10 mM MgCl2, 1xRoche
864 Complete Protease Inhibitor mixture) and different concentration of MBZ at room
865 temperature and vortexed for 1 hour. The reactions were terminated by 20 mM EDTA,
866 and the proteins were alkylated by 1.5 μL of 50 mM PNBM (CAYMAN CHEMICAL CO,
867 Cat. 21456-1) at room temperature and vortexed for 2 hours. This step was terminated
868 by denaturing in NuPAGE™ LDS Sample Buffer and 1x NuPAGE™ Sample Reducing
869 Agent (Invitrogen™). Samples were subjected to SDS-PAGE. The phosphorylation status
870 of MBP, CTR1-KD and MPK4 were analyzed by western blot using Recombinant Anti-
871 Thiophosphate ester antibody (Abcam, Cat. Ab92570, 1:5000).
872

873 **Statistical analysis**

874 A two-sided Student's t-test was used for comparisons of two conditions. The comparison
875 of meristem length, mature cell length, root length, GSA between multiple treatments or
876 genotypes was performed by One-way ANOVA and *post hoc* Tukey testing. Detailed
877 information was prepared in figure legends. Statistical significance of overlap between
878 DEGs from MBZ treatment and ethylene treatment was assessed by hypergeometric
879 distribution test.
880

881 **Data availability**

882 Data that support the findings of this study have been deposited in GEO. The GEO
883 number is GSE201648 .
884

885 **References**

886 Alexa, A., Rahnenfuhrer, J., and Lengauer, T. (2006). Improved scoring of functional
887 groups from gene expression data by decorrelating GO graph structure. Bioinformatics
888 22, 1600-1607.
889 Allen, J.J., Li, M., Brinkworth, C.S., Paulson, J.L., Wang, D., Hubner, A., Chou, W.H.,
890 Davis, R.J., Burlingame, A.L., Messing, R.O., et al. (2007). A semisynthetic epitope for
891 kinase substrates. Nat Methods 4, 511-516.
892 Alonso, J.M., Hirayama, T., Roman, G., Nourizadeh, S., and Ecker, J.R. (1999). EIN2, a
893 bifunctional transducer of ethylene and stress responses in Arabidopsis. Science 284,
894 2148-2152.
895 Alonso, J.M., Stepanova, A.N., Solano, R., Wisman, E., Ferrari, S., Ausubel, F.M., and
896 Ecker, J.R. (2003). Five components of the ethylene-response pathway identified in a
897 screen for weak ethylene-insensitive mutants in Arabidopsis. Proc Natl Acad Sci U S A
898 100, 2992-2997.

899 An, F., Zhao, Q., Ji, Y., Li, W., Jiang, Z., Yu, X., Zhang, C., Han, Y., He, W., Liu, Y., et
900 al. (2010). Ethylene-induced stabilization of ETHYLENE INSENSITIVE3 and EIN3-
901 LIKE1 is mediated by proteasomal degradation of EIN3 binding F-box 1 and 2 that
902 requires EIN2 in Arabidopsis. Plant Cell 22, 2384-2401.
903 Ariey-Bonnet, J., Carrasco, K., Le Grand, M., Hoffer, L., Betzi, S., Feracci, M., Tsvetkov,
904 P., Devred, F., Collette, Y., Morelli, X., et al. (2020). In silico molecular target prediction
905 unveils mebendazole as a potent MAPK14 inhibitor. Mol Oncol 14, 3083-3099.
906 Babicki, S., Arndt, D., Marcu, A., Liang, Y.J., Grant, J.R., Maciejewski, A., and Wishart,
907 D.S. (2016). Heatmapper: web-enabled heat mapping for all. Nucleic Acids Res 44,
908 W147-W153.
909 Berardini, T.Z., Reiser, L., Li, D.H., Mezheritsky, Y., Muller, R., Strait, E., and Huala, E.
910 (2015). The arabidopsis information resource: Making and mining the "gold standard"
911 annotated reference plant genome. Genesis 53, 474-485.
912 Chang, C., Kwok, S.F., Bleecker, A.B., and Meyerowitz, E.M. (1993). Arabidopsis
913 ethylene-response gene ETR1: similarity of product to two-component regulators.
914 Science 262, 539-544.
915 Chang, K.N., Zhong, S., Weirauch, M.T., Hon, G., Pelizzola, M., Li, H., Huang, S.S.C.,
916 Schmitz, R.J., Urich, M.A., Kuo, D., et al. (2013). Temporal transcriptional response to
917 ethylene gas drives growth hormone cross-regulation in Arabidopsis. Elife 2.
918 Chao, Q., Rothenberg, M., Solano, R., Roman, G., Terzaghi, W., and Ecker, J.R.
919 (1997). Activation of the ethylene gas response pathway in Arabidopsis by the nuclear
920 protein ETHYLENE-INSENSITIVE3 and related proteins. Cell 89, 1133-1144.
921 De Cnodder, T., Vissenberg, K., Van Der Straeten, D., and Verbelen, J.P. (2005).
922 Regulation of cell length in the Arabidopsis thaliana root by the ethylene precursor 1-
923 aminocyclopropane- 1-carboxylic acid: a matter of apoplastic reactions. The New
924 phytologist 168, 541-550.
925 Dobin, A., Davis, C.A., Schlesinger, F., Drenkow, J., Zaleski, C., Jha, S., Batut, P.,
926 Chaisson, M., and Gingeras, T.R. (2013). STAR: ultrafast universal RNA-seq aligner.
927 Bioinformatics 29, 15-21.
928 Feng, Y., Xu, P., Li, B., Li, P., Wen, X., An, F., Gong, Y., Xin, Y., Zhu, Z., Wang, Y., et
929 al. (2017). Ethylene promotes root hair growth through coordinated EIN3/EIL1 and
930 RHD6/RSL1 activity in Arabidopsis. Proc Natl Acad Sci U S A 114, 13834-13839.
931 Fu, L.W., Liu, Y.L., Qin, G.C., Wu, P., Zi, H.L., Xu, Z.T., Zhao, X.D., Wang, Y., Li, Y.X.,
932 Yang, S.H., et al. (2021). The TOR-EIN2 axis mediates nuclear signalling to modulate
933 plant growth. Nature 591, 288-292.
934 Furutani, M., and Morita, M.T. (2021). LAZY1-LIKE-mediated gravity signaling pathway
935 in root gravitropic set-point angle control. Plant Physiology 187, 1087-1095.
936 Ge, L.F., and Chen, R.J. (2016). Negative gravitropism in plant roots. Nature plants 2.
937 Guo, H., and Ecker, J.R. (2003). Plant responses to ethylene gas are mediated by
938 SCF(EBF1/EBF2)-dependent proteolysis of EIN3 transcription factor. Cell 115, 667-677.
939 Guseman, J.M., Webb, K., Srinivasan, C., and Dardick, C. (2017). DRO1 influences root
940 system architecture in Arabidopsis and Prunus species. Plant J 89, 1093-1105.
941 Guzman, P., and Ecker, J.R. (1990). Exploiting the triple response of Arabidopsis to
942 identify ethylene-related mutants. Plant Cell 2, 513-523.
943 He, W.R., Brumos, J., Li, H.J., Ji, Y.S., Ke, M., Gong, X.Q., Zeng, Q.L., Li, W.Y., Zhang,
944 X.Y., An, F.Y., et al. (2011). A Small-Molecule Screen Identifies L-Kynurenine as a

945 Competitive Inhibitor of TAA1/TAR Activity in Ethylene-Directed Auxin Biosynthesis and
946 Root Growth in Arabidopsis. Plant Cell 23, 3944-3960.
947 Hua, J., Sakai, H., Nourizadeh, S., Chen, Q.G., Bleecker, A.B., Ecker, J.R., and
948 Meyerowitz, E.M. (1998). EIN4 and ERS2 are members of the putative ethylene
949 receptor gene family in Arabidopsis. Plant Cell 10, 1321-1332.
950 Ju, C., Van de Poel, B., Cooper, E.D., Thierer, J.H., Gibbons, T.R., Delwiche, C.F., and
951 Chang, C. (2015). Conservation of ethylene as a plant hormone over 450 million years
952 of evolution. Nature plants 1, 14004.
953 Ju, C., Yoon, G.M., Shemansky, J.M., Lin, D.Y., Ying, Z.I., Chang, J., Garrett, W.M.,
954 Kessenbrock, M., Groth, G., Tucker, M.L., et al. (2012). CTR1 phosphorylates the
955 central regulator EIN2 to control ethylene hormone signaling from the ER membrane to
956 the nucleus in Arabidopsis. Proc Natl Acad Sci U S A 109, 19486-19491.
957 Kieber, J.J., Rothenberg, M., Roman, G., Feldmann, K.A., and Ecker, J.R. (1993).
958 CTR1, a negative regulator of the ethylene response pathway in Arabidopsis, encodes a
959 member of the raf family of protein kinases. Cell 72, 427-441.
960 Le, J., Vandenbussche, F., Van Der Straeten, D., and Verbelen, J.P. (2001). In the early
961 response of Arabidopsis roots to ethylene, cell elongation is up- and down-regulated
962 and uncoupled from differentiation. Plant Physiol 125, 519-522.
963 Li, W., Lacey, R.F., Ye, Y., Lu, J., Yeh, K.C., Xiao, Y., Li, L., Wen, C.K., Binder, B.M.,
964 and Zhao, Y. (2017). Triplin, a small molecule, reveals copper ion transport in ethylene
965 signaling from ATX1 to RAN1. PLoS Genet 13, e1006703.
966 Liao, C.Y., Smet, W., Brunoud, G., Yoshida, S., Vernoux, T., and Weijers, D. (2015a).
967 Reporters for sensitive and quantitative measurement of auxin response. Nat Methods
968 12, 207-210, 202 p following 210.
969 Liao, C.Y., Smet, W., Brunoud, G., Yoshida, S., Vernoux, T., and Weijers, D. (2015b).
970 Reporters for sensitive and quantitative measurement of auxin response (vol 12, pg
971 207, 2015). Nat Methods 12, 1098-1098.
972 Liao, C.Y., Smet, W., Brunoud, G., Yoshida, S., Vernoux, T., and Weijers, D. (2015).
973 Reporters for sensitive and quantitative measurement of auxin response. Nat Methods
974 12, 207-210, 202 p following 210.
975 Lynch, J.P. (2019). Root phenotypes for improved nutrient capture: an underexploited
976 opportunity for global agriculture. New Phytol 223, 548-564.
977 Mayerhofer, H., Mueller-Dieckmann, C., and Mueller-Dieckmann, J. (2011). Cloning,
978 expression, purification and preliminary X-ray analysis of the protein kinase domain of
979 constitutive triple response 1 (CTR1) from Arabidopsis thaliana. Acta Crystallogr Sect F
980 Struct Biol Cryst Commun 67, 117-120.
981 Mayerhofer, H., Panneerselvam, S., and Mueller-Dieckmann, J. (2012). Protein kinase
982 domain of CTR1 from Arabidopsis thaliana promotes ethylene receptor cross talk. J Mol
983 Biol 415, 768-779.
984 Mou, W., Kao, Y.T., Michard, E., Simon, A.A., Li, D., Wudick, M.M., Lizzio, M.A., Feijo,
985 J.A., and Chang, C. (2020). Ethylene-independent signaling by the ethylene precursor
986 ACC in Arabidopsis ovular pollen tube attraction. Nat Commun 11, 4082.
987 Muller, M., and Munne-Bosch, S. (2015). Ethylene Response Factors: A Key Regulatory
988 Hub in Hormone and Stress Signaling. Plant Physiol 169, 32-41.

Nakamura, M., Naoi, K., Shoji, T., and Hashimoto, T. (2004). Low concentrations of propyzamide and oryzalin alter microtubule dynamics in Arabidopsis epidermal cells. Plant Cell Physiol 45, 1330-1334.
Negi, S., Ivanchenko, M.G., and Muday, G.K. (2008). Ethylene regulates lateral root formation and auxin transport in Arabidopsis thaliana. Plant J 55, 175-187.
Ogura, T., Goeschl, C., and Busch, W. (2022). A Multiplexed, Time-Resolved Assay of Root Gravitropic Bending on Agar Plates. Methods Mol Biol 2368, 61-70.
Pattyn, J., Vaughan-Hirsch, J., and Van de Poel, B. (2021). The regulation of ethylene biosynthesis: a complex multilevel control circuitry. New Phytol 229, 770-782.
Pettersen, E.F., Goddard, T.D., Huang, C.C., Couch, G.S., Greenblatt, D.M., Meng, E.C., and Ferrin, T.E. (2004). UCSF Chimera--a visualization system for exploratory research and analysis. J Comput Chem 25, 1605-1612.
Poirier, V., Roumet, C., and Munson, A.D. (2018). The root of the matter: Linking root traits and soil organic matter stabilization processes. Soil Biology and Biochemistry 120, 246-259.
Qiao, H., Shen, Z., Huang, S.S., Schmitz, R.J., Urich, M.A., Briggs, S.P., and Ecker, J.R. (2012a). Processing and subcellular trafficking of ER-tethered EIN2 control response to ethylene gas. Science 338, 390-393.
Qiao, H., Shen, Z.X., Huang, S.S.C., Schmitz, R.J., Urich, M.A., Briggs, S.P., and Ecker, J.R. (2012b). Processing and Subcellular Trafficking of ER-Tethered EIN2 Control Response to Ethylene Gas. Science 338, 390-393.
Robinson, M.D., McCarthy, D.J., and Smyth, G.K. (2010). edgeR: a Bioconductor package for differential expression analysis of digital gene expression data. Bioinformatics 26, 139-140.
Rosquete, M.R., von Wangenheim, D., Marhavy, P., Barbez, E., Stelzer, E.H., Benkova, E., Maizel, A., and Kleine-Vehn, J. (2013a). An auxin transport mechanism restricts positive orthogravitropism in lateral roots. Current biology : CB 23, 817-822.
Rosquete, M.R., von Wangenheim, D., Marhavy, P., Barbez, E., Stelzer, E.H.K., Benkova, E., Maizel, A., and Kleine-Vehn, J. (2013b). An Auxin Transport Mechanism Restricts Positive Orthogravitropism in Lateral Roots. Curr Biol 23, 817-822.
Rosquete, M.R., von Wangenheim, D., Marhavy, P., Barbez, E., Stelzer, E.H., Benkova, E., Maizel, A., and Kleine-Vehn, J. (2013). An auxin transport mechanism restricts positive orthogravitropism in lateral roots. Current biology : CB 23, 817-822.
Roychoudhry, S., Del Bianco, M., Kieffer, M., and Kepinski, S. (2013). Auxin controls gravitropic setpoint angle in higher plant lateral branches. Current biology : CB 23, 1497-1504.
S F Yang, a., and Hoffman, N.E. (1984). Ethylene Biosynthesis and its Regulation in Higher Plants. Annual Review of Plant Physiology 35, 155-189.
Sakai, H., Hua, J., Chen, Q.G., Chang, C., Medrano, L.J., Bleecker, A.B., and Meyerowitz, E.M. (1998). ETR2 is an ETR1-like gene involved in ethylene signaling in Arabidopsis. Proc Natl Acad Sci U S A 95, 5812-5817.
Schindelin, J., Arganda-Carreras, I., Frise, E., Kaynig, V., Longair, M., Pietzsch, T., Preibisch, S., Rueden, C., Saalfeld, S., Schmid, B., et al. (2012). Fiji: an open-source platform for biological-image analysis. Nat Methods 9, 676-682.

1033 Sun, X.Z., Li, Y.X., He, W.R., Ji, C.G., Xia, P.X., Wang, Y.C., Du, S., Li, H.J., Raikhel,
1034 N., Xiao, J.Y., et al. (2017). Pyrazinamide and derivatives block ethylene biosynthesis
1035 by inhibiting ACC oxidase. Nat Commun 8.
1036 Trott, O., and Olson, A.J. (2010). AutoDock Vina: improving the speed and accuracy of
1037 docking with a new scoring function, efficient optimization, and multithreading. J Comput
1038 Chem 31, 455-461.
1039 Uga, Y., Sugimoto, K., Ogawa, S., Rane, J., Ishitani, M., Hara, N., Kitomi, Y., Inukai, Y.,
1040 Ono, K., Kanno, N., et al. (2013). Control of root system architecture by DEEPER
1041 ROOTING 1 increases rice yield under drought conditions. Nature genetics 45, 1097-
1042 1102.
1043 Vaseva, II, Qudeimat, E., Potuschak, T., Du, Y., Genschik, P., Vandenbussche, F., and
1044 Van Der Straeten, D. (2018). The plant hormone ethylene restricts Arabidopsis growth
1045 via the epidermis. Proc Natl Acad Sci U S A 115, E4130-E4139.
1046 Waidmann, S., Rosquete, M.R., Scholler, M., Sarkel, E., Lindner, H., LaRue, T., Petrik,
1047 I., Dunser, K., Martopawiro, S., Sasidharan, R., et al. (2019a). Cytokinin functions as an
1048 asymmetric and anti-gravitropic signal in lateral roots. Nat Commun 10.
1049 Waidmann, S., Ruiz Rosquete, M., Scholler, M., Sarkel, E., Lindner, H., LaRue, T.,
1050 Petrik, I., Dunser, K., Martopawiro, S., Sasidharan, R., et al. (2019b). Cytokinin
1051 functions as an asymmetric and anti-gravitropic signal in lateral roots. Nat Commun 10,
1052 3540.
1053 Waidmann, S., Ruiz Rosquete, M., Scholler, M., Sarkel, E., Lindner, H., LaRue, T.,
1054 Petrik, I., Dunser, K., Martopawiro, S., Sasidharan, R., et al. (2019). Cytokinin functions
1055 as an asymmetric and anti-gravitropic signal in lateral roots. Nat Commun 10, 3540.
1056 Waite, J.M., and Dardick, C. (2021). The roles of the IGT gene family in plant
1057 architecture: past, present, and future. Curr Opin Plant Biol 59.
1058 Wen, X., Zhang, C., Ji, Y., Zhao, Q., He, W., An, F., Jiang, L., and Guo, H. (2012).
1059 Activation of ethylene signaling is mediated by nuclear translocation of the cleaved EIN2
1060 carboxyl terminus. Cell Res 22, 1613-1616.
1061 Xiao, G., and Zhang, Y. (2020). Adaptive Growth: Shaping Auxin-Mediated Root
1062 System Architecture. Trends in plant science 25, 121-123.
1063 Yoshihara, T., and Spalding, E.P. (2017). LAZY Genes Mediate the Effects of Gravity
1064 on Auxin Gradients and Plant Architecture. Plant Physiology 175, 959-969.
1065 Zhu, Y., Li, H.J., Su, Q., Wen, J., Wang, Y.F., Song, W., Xie, Y.P., He, W.R., Yang, Z.,
1066 Jiang, K., et al. (2019). A phenotype-directed chemical screen identifies ponalrestat as
1067 an inhibitor of the plant flavin monooxygenase YUCCA in auxin biosynthesis. J Biol
1068 Chem 294, 19923-19933.
1069 Zurcher, E., Tavor-Deslex, D., Lituiev, D., Enkerli, K., Tarr, P.T., and Muller, B. (2013).
1070 A robust and sensitive synthetic sensor to monitor the transcriptional output of the
1071 cytokinin signaling network in planta. Plant Physiol 161, 1066-1075.
1072

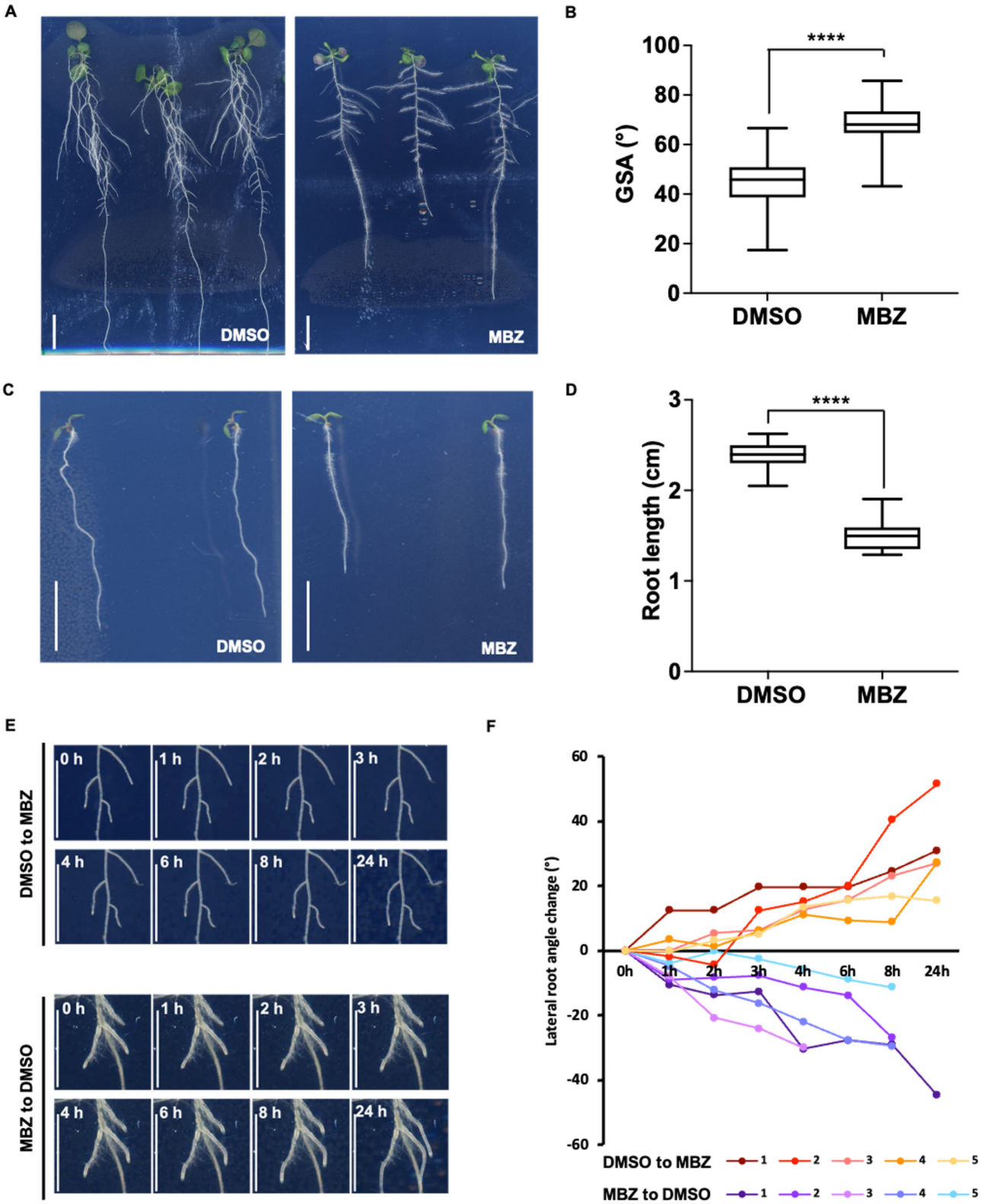

Figure 1. MBZ treatment perturbs root system architecture (RSA).

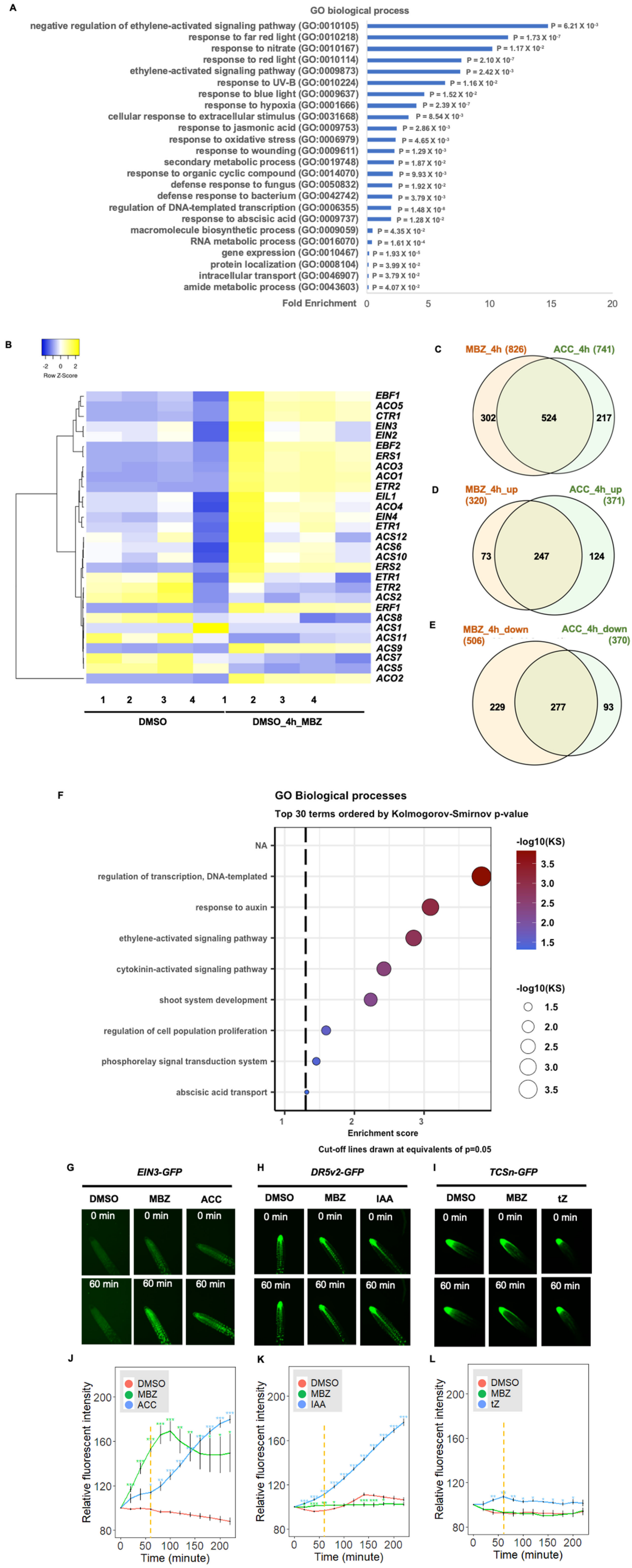

Figure 2. MBZ treatment regulates the ethylene pathway.

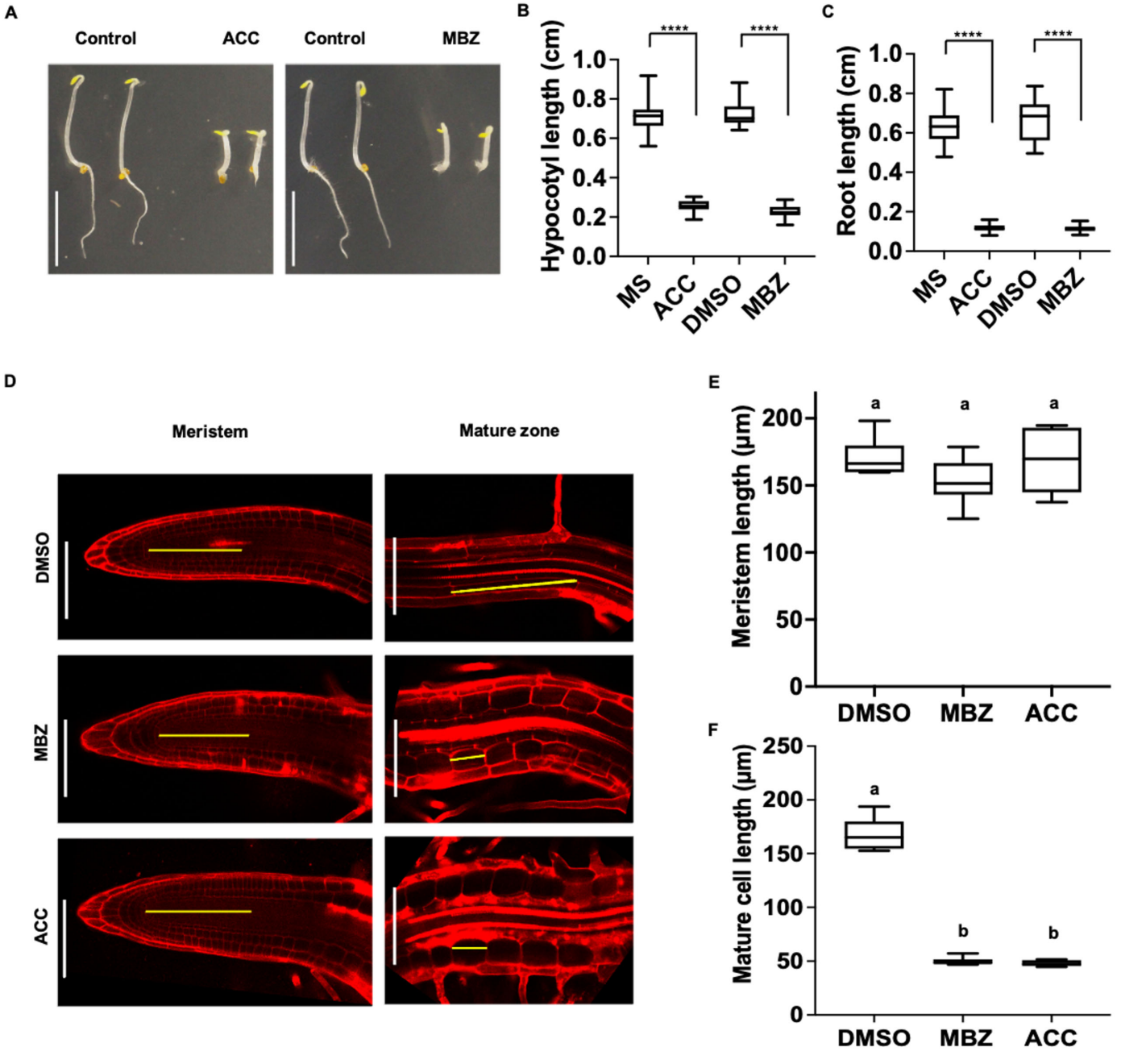

Figure 3. MBZ induces ethylene response and mimics ACC treatment

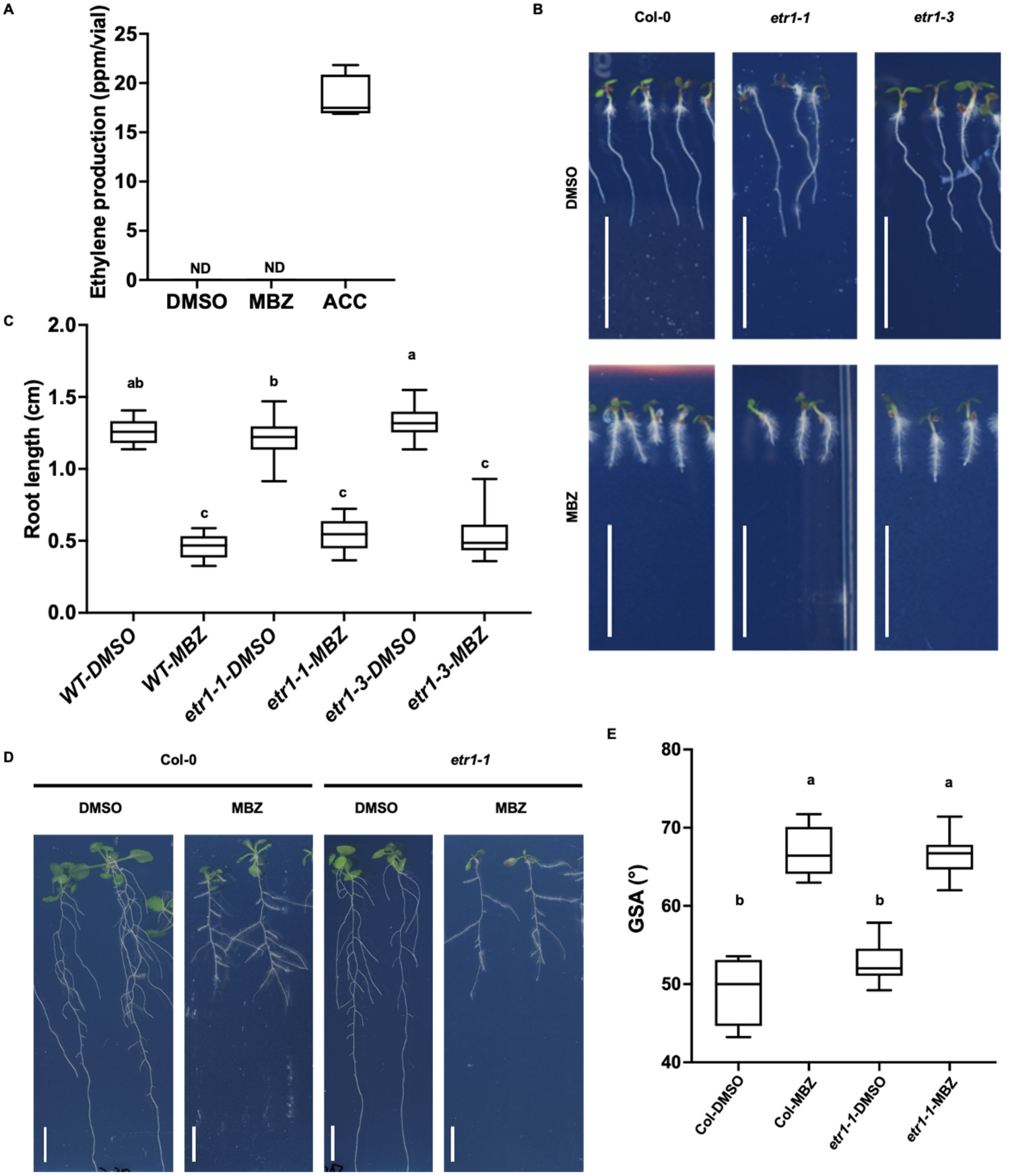

Figure 4. MBZ acts downstream of ethylene biosynthesis

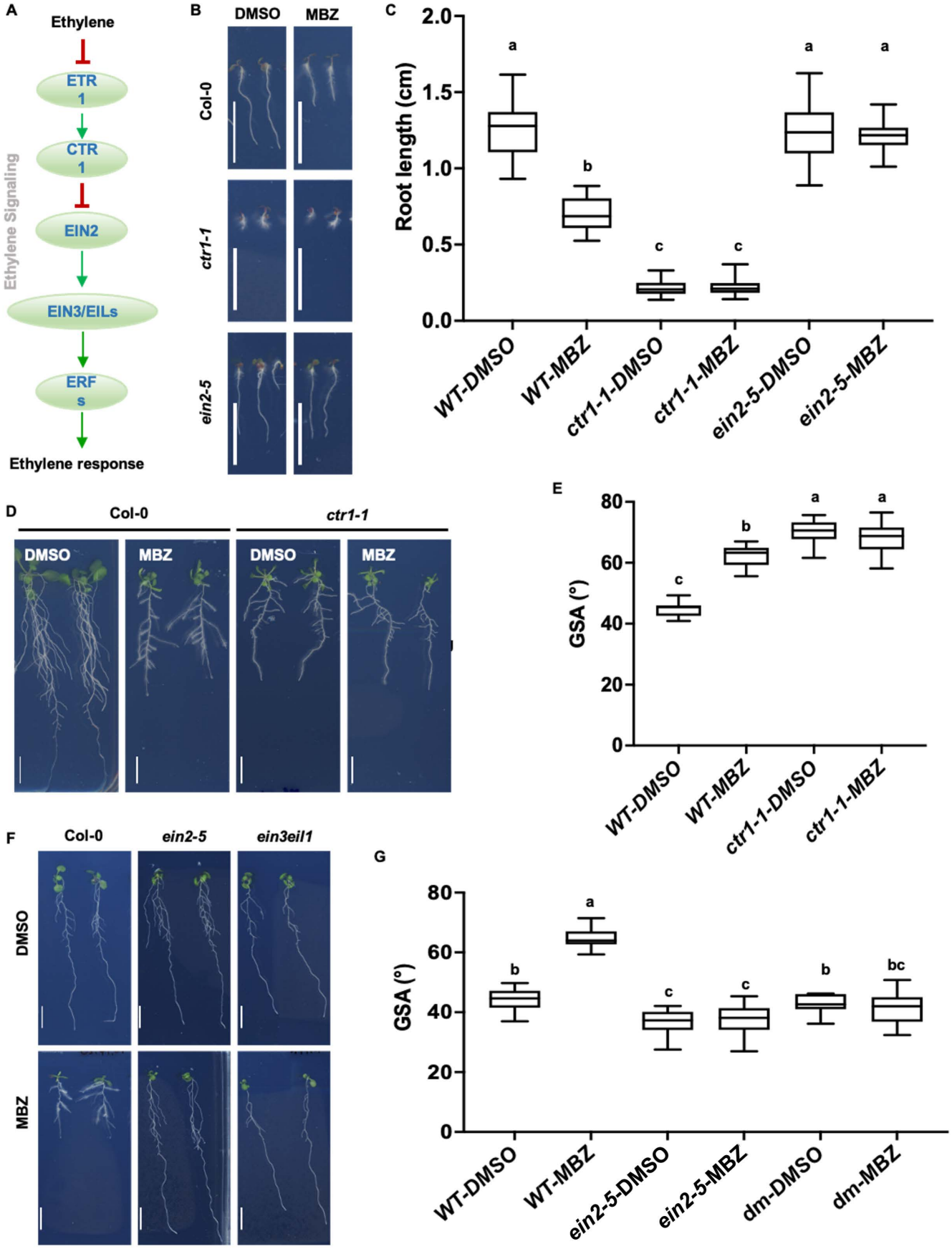

Figure 5. MBZ targets the ethylene signaling pathway

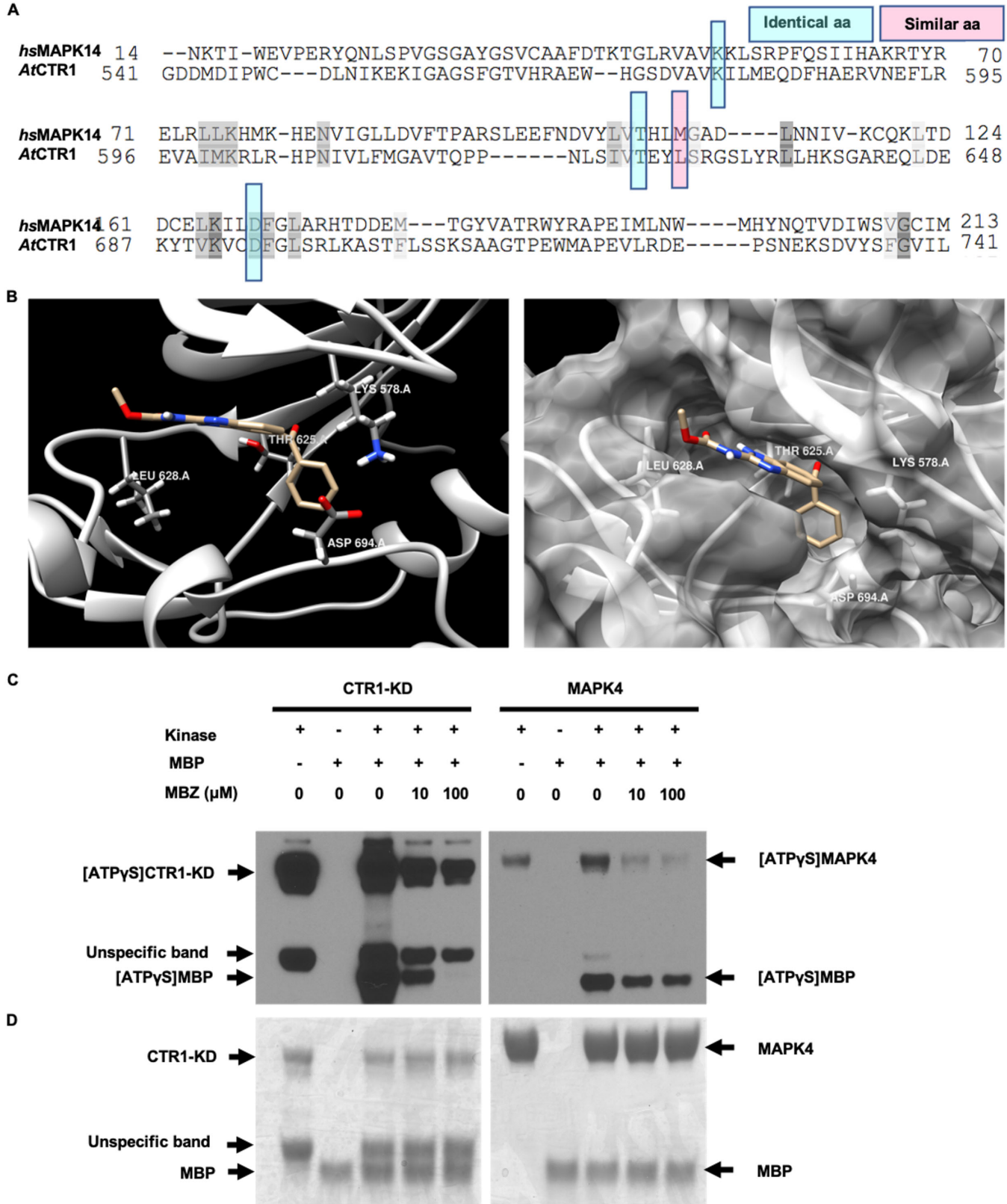

Figure 6. MBZ inhibits CTR1 kinase activity

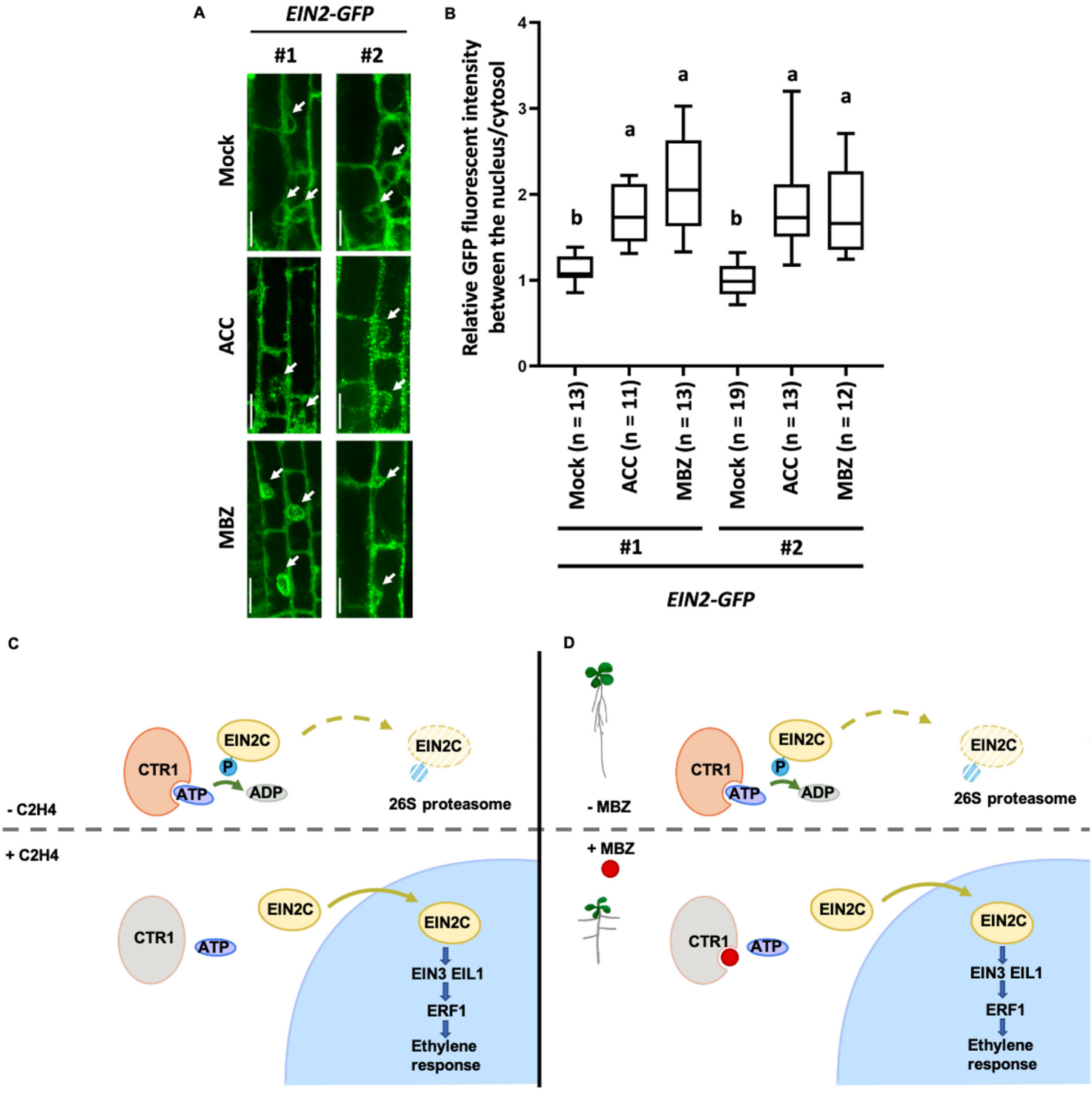

Figure 7. MBZ activates ethylene signaling

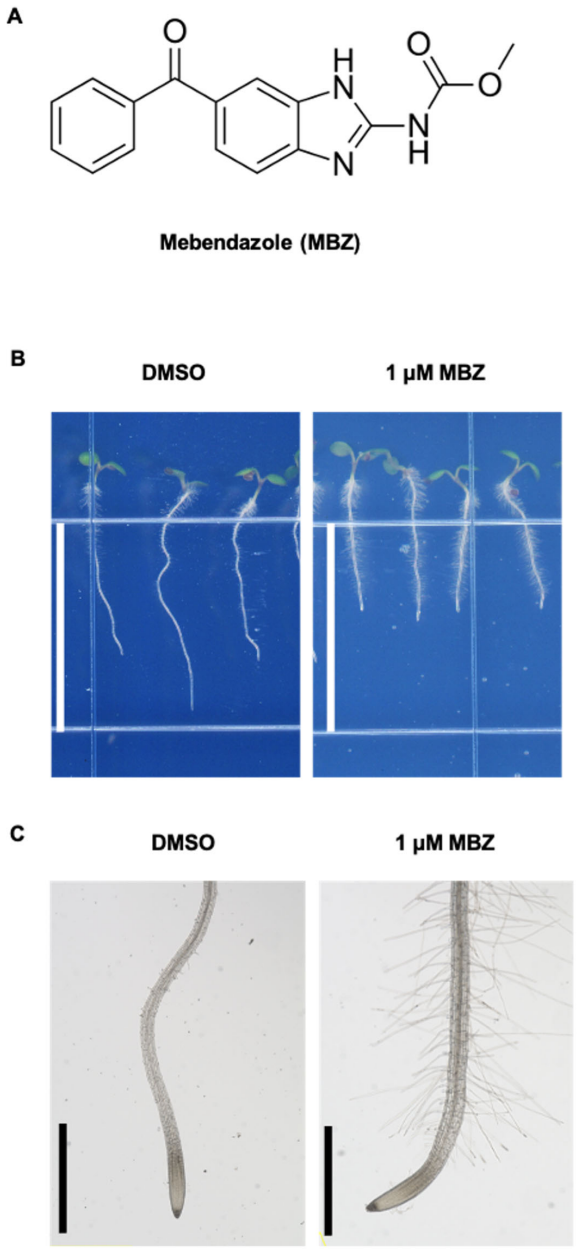

Figure S1. MBZ treatment affects root growth and development

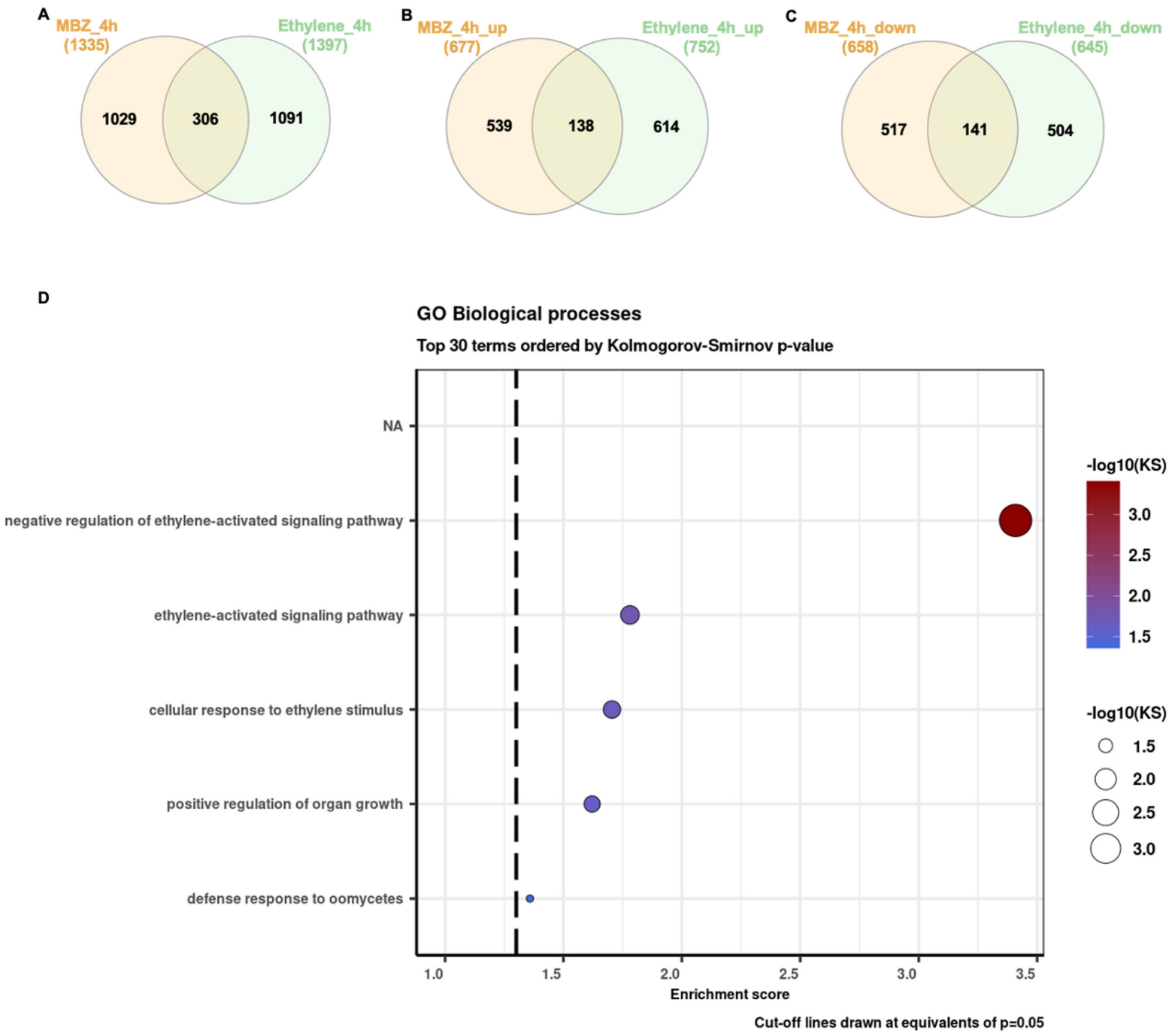

Figure S2. The analysis of differentially expressed genes (DEGs) by MBZ treatment.

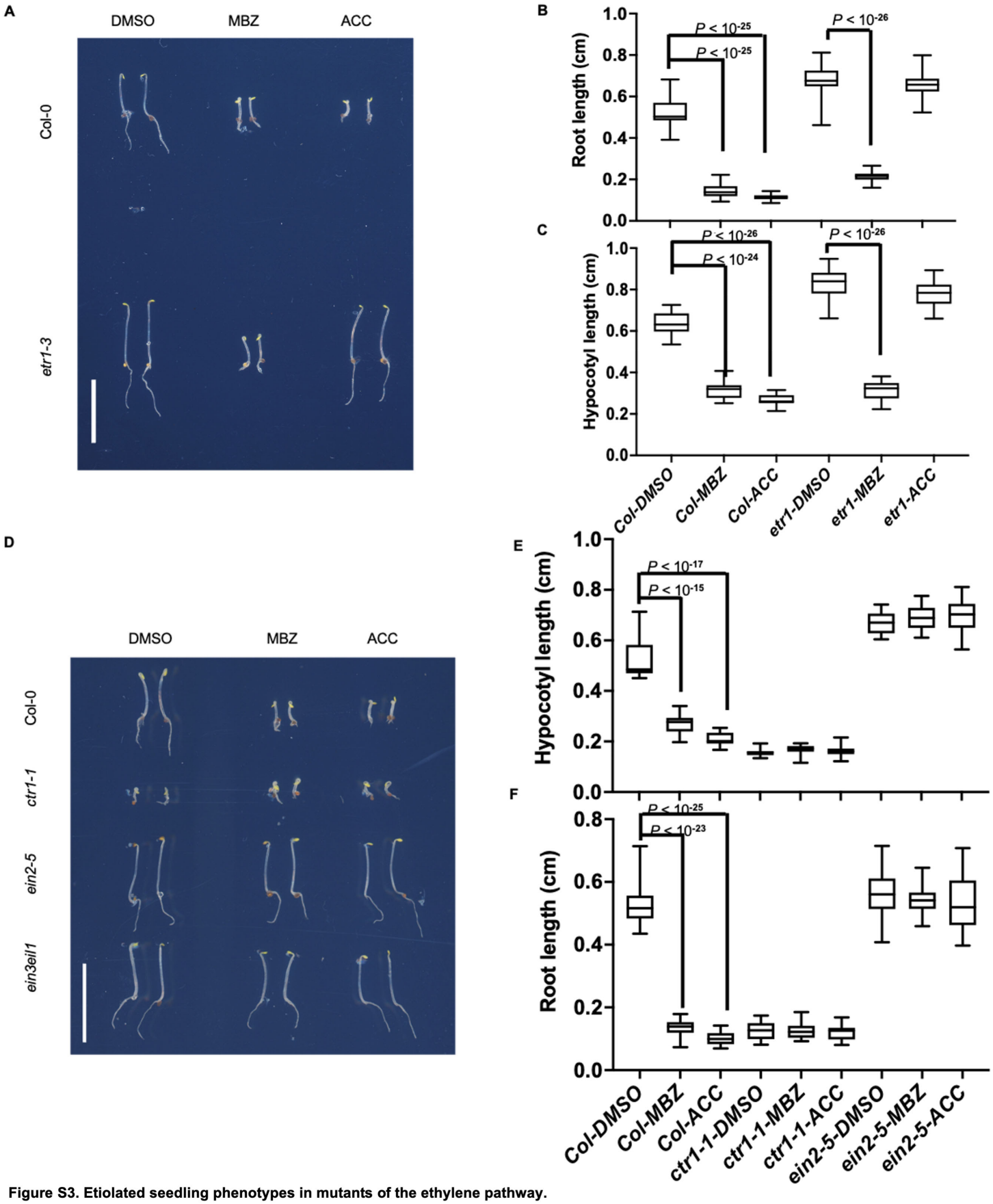

Figure S3. Etiolated seedling phenotypes in mutants of the ethylene pathway.

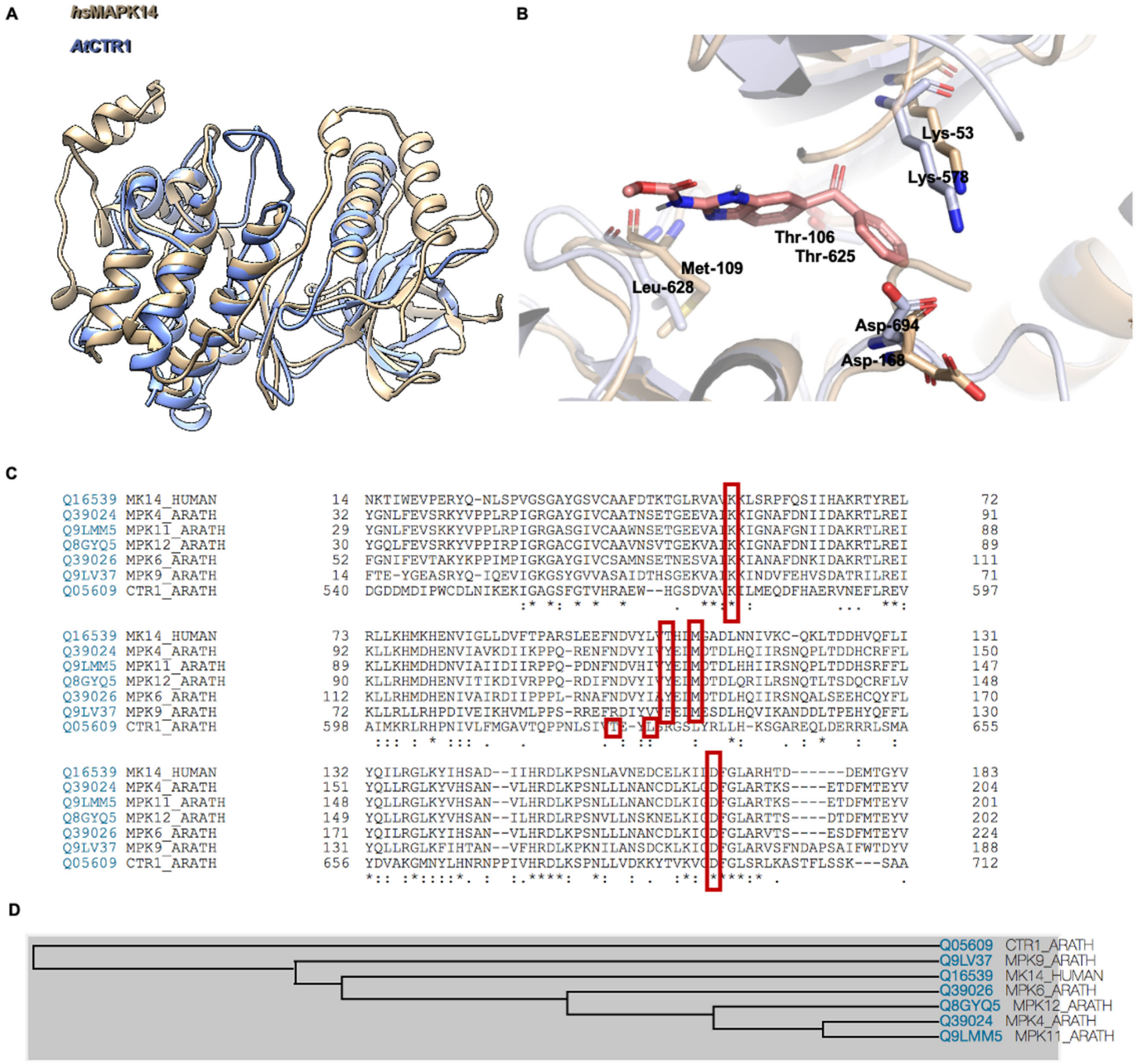

Figure S4. Alignment of *At*CTR1-KD and *hs*MAPK14

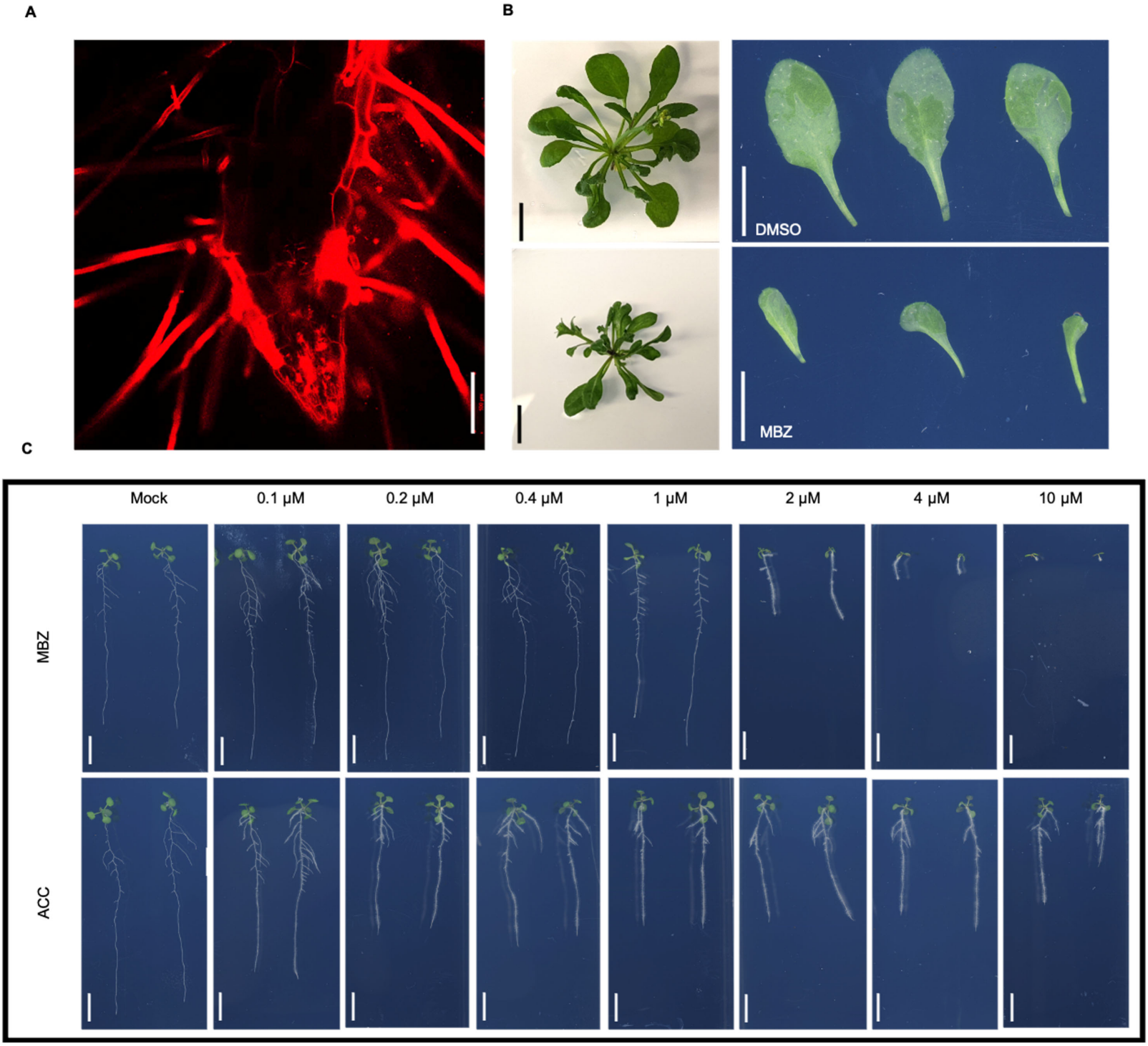

Figure S5. High concentrations or long-term treatment of MBZ induce phenotypes that go beyond ethylene induced effects

Table S1. The list of blast hits in Arabidopsis using the MAPK14_human sequence as BLASTP

JVD9H54701R-Alignment-Descriptions

Description	Scientific Name	Max Score	Total Score	Query Cover	E value	Per. ident	Acc. Len	Accession
MAP kinase 4 [Arabidopsis thaliana]	Arabidopsis thaliana	346	346	93%	3E-117	51.18	376	NP_192046.1
mitogen-activated protein kinase 4 [Arabidopsis thaliana]	Arabidopsis thaliana	346	346	93%	3E-117	51.18	376	ABR46146.1
mitogen-activated protein kinase 4 [Arabidopsis thaliana]	Arabidopsis thaliana	345	345	93%	8E-117	50.88	376	ABR46148.1
MAP kinase [Arabidopsis thaliana]	Arabidopsis thaliana	345	345	93%	9E-117	50.88	376	BAA04867.1
mitogen-activated protein kinase 4 [Arabidopsis thaliana]	Arabidopsis thaliana	344	344	93%	1E-116	50.88	376	ABR46162.1
unnamed protein product [Arabidopsis thaliana]	Arabidopsis thaliana	340	340	95%	8E-115	47.71	376	VYS62299.1
MPK5 [Arabidopsis thaliana]	Arabidopsis thaliana	339	339	95%	9E-115	47.71	376	OAO98154.1
MAP kinase 11 [Arabidopsis thaliana]	Arabidopsis thaliana	337	337	93%	6E-114	49.71	369	NP_001117210.1
unnamed protein product [Arabidopsis thaliana]	Arabidopsis thaliana	337	337	93%	6E-114	49.71	369	CAA0154293.1
MAP kinase 5 [Arabidopsis thaliana]	Arabidopsis thaliana	337	337	95%	8E-114	47.43	376	NP_567378.4
unnamed protein product [Arabidopsis thaliana]	Arabidopsis thaliana	336	336	95%	2E-113	46.84	370	CAD5324945.1
MAP kinase [Arabidopsis thaliana]	Arabidopsis thaliana	335	335	95%	2E-113	46.55	370	BAA04866.1
mitogen-activated protein kinase 3 [Arabidopsis thaliana]	Arabidopsis thaliana	335	335	95%	2E-113	46.55	370	NP_190150.1
MAP kinase [Arabidopsis thaliana]	Arabidopsis thaliana	330	330	95%	3E-111	46.57	376	BAA04868.1
mitogen-activated protein kinase 12 [Arabidopsis thaliana]	Arabidopsis thaliana	329	329	92%	9E-111	49.26	372	NP_182131.2
mitogen-activated protein kinase 12 [Arabidopsis thaliana]	Arabidopsis thaliana	330	330	92%	2E-110	49.26	406	NP_001325006.1
Mitogen-activated protein kinase 6 [Arabidopsis thaliana]	Arabidopsis thaliana	323	323	95%	2E-108	46.84	364	6DTL_A
Crystal structure of Arabidopsis thaliana MPK6 [Arabidopsis thaliana]	Arabidopsis thaliana	323	323	95%	3E-108	46.84	370	5CI6_A
unnamed protein product [Arabidopsis thaliana]	Arabidopsis thaliana	323	323	92%	3E-108	46.31	393	VYS60924.1
MAP kinase 6 [Arabidopsis thaliana]	Arabidopsis thaliana	323	323	95%	4E-108	46.84	395	NP_181907.1
MAP kinase 10 [Arabidopsis thaliana]	Arabidopsis thaliana	323	323	92%	4E-108	46.31	393	NP_191538.1
unnamed protein product [Arabidopsis thaliana]	Arabidopsis thaliana	323	323	92%	5E-108	46.31	393	CAA0387508.1
MPK10 [Arabidopsis thaliana]	Arabidopsis thaliana	323	323	92%	6E-108	46.31	393	OAP05435.1
unnamed protein product [Arabidopsis thaliana]	Arabidopsis thaliana	321	321	92%	2E-107	46.02	393	CAD5326291.1
MAP kinase [Arabidopsis thaliana]	Arabidopsis thaliana	318	318	95%	2E-106	46.29	373	CAB51417.1
Protein kinase superfamily protein [Arabidopsis thaliana]	Arabidopsis thaliana	317	317	92%	4E-106	47.79	363	NP_001030990.1
unnamed protein product [Arabidopsis thaliana]	Arabidopsis thaliana	316	316	92%	8E-106	47.79	363	CAD5312051.1
mitogen-activated protein kinase homolog 2 [Arabidopsis thaliana]	Arabidopsis thaliana	316	316	85%	2E-105	49.68	376	NP_564746.1
ATMPK1 [Arabidopsis thaliana]	Arabidopsis thaliana	315	315	93%	2E-105	46.33	370	BAA03535.1
unnamed protein product [Arabidopsis thaliana]	Arabidopsis thaliana	315	315	93%	3E-105	46.33	370	CAA0186271.1
AT1G10210 [Arabidopsis thaliana]	Arabidopsis thaliana	315	315	93%	3E-105	46.33	370	BAH19911.1
mitogen-activated protein kinase 1 [Arabidopsis thaliana]	Arabidopsis thaliana	315	315	93%	3E-105	46.33	370	NP_001031017.1
mitogen-activated protein kinase 14 [Arabidopsis thaliana]	Arabidopsis thaliana	315	315	95%	3E-105	45.04	361	NP_195363.1
ATMPK2 [Arabidopsis thaliana]	Arabidopsis thaliana	315	315	85%	4E-105	49.35	376	BAA03536.1
unnamed protein product [Arabidopsis thaliana]	Arabidopsis thaliana	313	313	95%	1E-104	45.04	361	CAA0397686.1
MPK14 [Arabidopsis thaliana]	Arabidopsis thaliana	311	311	95%	8E-104	44.76	361	OAO98488.1
MAP kinase 5-CT [Arabidopsis thaliana]	Arabidopsis thaliana	310	310	81%	9E-104	50	337	ADZ76491.1
MAP kinase 7 [Arabidopsis thaliana]	Arabidopsis thaliana	310	310	85%	2E-103	48.71	368	NP_179409.1
MPK7 [Arabidopsis thaliana]	Arabidopsis thaliana	310	310	85%	2E-103	48.71	368	OAP11028.1
MAP Kinase [Arabidopsis thaliana]	Arabidopsis thaliana	309	309	86%	4E-103	50.48	354	AAB61033.1
unnamed protein product [Arabidopsis thaliana]	Arabidopsis thaliana	310	310	91%	4E-103	48.49	389	CAD5321516.1
unnamed protein product [Arabidopsis thaliana]	Arabidopsis thaliana	309	309	85%	5E-103	48.71	368	CAA0364931.1
MAP kinase 11 [Arabidopsis thaliana]	Arabidopsis thaliana	307	307	78%	2E-102	52.08	346	NP_001322112.1
MAP kinase [Arabidopsis thaliana]	Arabidopsis thaliana	306	306	85%	1E-101	48.06	368	BAA04870.1
unnamed protein product [Arabidopsis thaliana]	Arabidopsis thaliana	310	310	86%	3E-99	48.12	716	CAD5330118.1
mitogen-activated protein kinase 12 [Arabidopsis thaliana]	Arabidopsis thaliana	297	297	80%	5E-99	51.03	324	NP_001189755.1
mitogen-activated protein kinase 16 [Arabidopsis thaliana]	Arabidopsis thaliana	287	287	91%	7E-92	42.77	567	NP_197402.1
Unknown protein [Arabidopsis thaliana]	Arabidopsis thaliana	287	287	91%	7E-92	42.77	567	AAL32607.1
unnamed protein product [Arabidopsis thaliana]	Arabidopsis thaliana	287	287	91%	9E-92	42.77	569	CAD5332107.1
MAP kinase [Arabidopsis thaliana]	Arabidopsis thaliana	276	276	75%	6E-90	50	360	BAD 95376.10
putative MAP kinase [Arabidopsis thaliana]	Arabidopsis thaliana	271	271	90%	4E-87	42.6	431	AAK62464.1
MPK15 [Arabidopsis thaliana]	Arabidopsis thaliana	274	274	92%	1E-86	41.86	575	OAP17567.1
MAP kinase 19 [Arabidopsis thaliana]	Arabidopsis thaliana	268	268	91%	3E-86	42.18	425	NP_001326968.1
MAP kinase 15 [Arabidopsis thaliana]	Arabidopsis thaliana	272	272	92%	4E-86	41.86	576	NP_565070.2
MPK8 [Arabidopsis thaliana]	Arabidopsis thaliana	269	269	92%	1E-84	42.15	588	OAP18797.1